

# Stochastic Epidemic Models with Partial Information

Florent Ouabo Kamkumo · Ibrahim Mbouandi Njiasse · Ralf Wunderlich

Version of March 11, 2025

**Abstract** Mathematical models of epidemics often use compartmental models dividing the population into several compartments. Based on a microscopic setting describing the temporal evolution of the subpopulation sizes in the compartments by stochastic counting processes one can derive macroscopic models for large populations describing the average behavior by associated ordinary differential equations such as the celebrated SIR model. Further, diffusion approximations allow to address fluctuations from the average and to describe the state dynamics also for smaller populations by stochastic differential equations.

In general, not all state variables are directly observable, and we face the so-called "dark figure" problem, which concerns, for example, the unknown number of asymptomatic and undetected infections. The present study addresses this problem by developing stochastic epidemic models that incorporate partial information about the current state of the epidemic, also known as nowcast uncertainty. Examples include a simple extension of the SIR model, a model for a disease with lifelong immunity after infection or vaccination, and a Covid-19 model. For the latter, we propose a "cascade state approach" that allows to exploit the information contained in formally hidden compartments with observable inflow but unobservable outflow. Furthermore, parameter estimation and calibration are performed using ridge regression for the Covid-19 model. The results of the numerical simulations illustrate the theoretical findings.

**Keywords** Continuous-time Markov chain · Stochastic epidemic model · Stochastic differential equation · Diffusion approximation · Partial information · Covid-19 · Parameters estimation

**Mathematics Subject Classification (2010)** 60J25 · 60J60 · 92D30 · 92-10 · 62J07

## Contents

1	Introduction . . . . .	3
2	Microscopic Models . . . . .	6
2.1	Counting processes . . . . .	6
2.2	Adapted Gillespie Algorithm for CTMC Simulation . . . . .	7
3	Macroscopic Model . . . . .	9
3.1	Law of Large Numbers and ODE Models . . . . .	10
3.2	Central Limit Theorem . . . . .	12
3.3	Numerical Illustration of Limit Theorems . . . . .	12
3.4	Diffusion Approximation . . . . .	16
4	Models Examples . . . . .	17
4.1	$SI^{\pm}RS$ Model . . . . .	17
4.2	Measles Model . . . . .	19
4.3	Covid-19 Model . . . . .	23
4.4	Diffusion Approximation of Covid-19 Model . . . . .	26
4.5	Cascade State Modeling . . . . .	27
4.6	Covid-19 Modeling with Cascade States . . . . .	32
5	Data Set and Calibration . . . . .	34
5.1	Model Parameters . . . . .	35
5.2	Model Prediction . . . . .	39
6	Numerical Results . . . . .	40
6.1	Model Calibration . . . . .	40
6.2	Simulation of Covid-19 Model . . . . .	45
7	Conclusion . . . . .	47
A	List of Abbreviations . . . . .	47
B	List of Notations . . . . .	48
C	Model Dynamics . . . . .	50
C.1	Diffusion Approximation of Covid-19 Model without Cascade States . . . . .	51
C.2	Diffusion Approximation of Covid-19 Model with Cascade States - Continuous-Time . . . . .	52
C.3	Diffusion Approximation of Covid-19 Model with Cascade States - Discrete-Time . . . . .	53

## 1 Introduction

For many years, mathematical models have been an important tool for scientists to understand and analyze the dynamics of epidemics. Epidemics have always been a major public health challenge and require effective strategies to understand and control the spread of infectious diseases. Traditional deterministic models such as SIR, SIRS and SEIR have provided valuable insights into disease transmission and progression. Many researchers have developed deterministic epidemic models to assist public health officials in understanding the spread of infectious diseases. Kermack and McKendrick [34] introduced the deterministic SIR model, which today forms the basis of much modern epidemic modeling. Their work was originally motivated by epidemics of bubonic plague in India. The goal was to provide a mathematical explanation for observed epidemic behaviors, such as the rise and fall in the number of cases, using a theoretical framework that could guide public health interventions. Since then, numerous compartmental mathematical models, both deterministic and stochastic, have been developed to analyze and understand epidemic behavior across the world.

The underlying idea of these models is to divide the population into several subpopulations collected in the compartments. On a microscopic level the temporal evolution of the subpopulation sizes in the compartments are described by stochastic counting processes. Then one can derive macroscopic models for large populations describing the average behavior by associated ordinary differential equations (ODEs) such as the celebrated SIR model. For the fluctuations from the average that are interesting for smaller populations diffusion approximations can be derived. They describe the state dynamics by stochastic differential equations (SDEs). However, in general, some of the state variables are not directly observable since they consist of individuals with asymptomatic and non-detected infections. This is also known as “nowcast uncertainty” or the “dark figure” problem. Such not directly observable states are problematic if it comes to the computation of characteristics of the epidemic such as the effective reproduction rate and the prevalence of the infection within the population. Further, the management and containment of epidemics relying on solutions of stochastic optimal control problems and the associated feedback controls need observations of the current state as input.

This article addresses the above problems with not directly observable or hidden states of an epidemics and proposes stochastic epidemic models that incorporate partial information about the current state of the epidemic. They are used in the companion papers [46] for estimating the hidden states based on the available information from observable states, and [42] for solving stochastic optimal control problems under partial information arising from the decision problem of a social planner seeking cost-optimal containment of an epidemic.

**Literature review on Deterministic Epidemic Model.** Ahmad et al. [3] introduce a deterministic mathematical model to represent the dynamics of human-to-human transmission of the monkeypox virus, integrating post-exposure vaccination, pre-exposure vaccination, and isolation strategies. The post-exposure vaccination targets susceptible individuals, while the pre-exposure vaccination is administered to asymptomatic individuals. Later Dounia B. et al. [40] presents a SEIR epidemic model designed to capture the transmission dynamics of the Central and West African clades of monkeypox. The authors focus on model properties such as boundedness, positivity, and other stability characteristics of solutions. They then formulate a deterministic optimal control problem with the objec-

tive of determining the best strategies to significantly reduce transmission or eradicate the disease. Mehmet G. and Kemal T. [27] utilize a deterministic SIR epidemic model to simulate and forecast the spread of the Hepatitis B virus. They provide a comprehensive and detailed analysis of the model and illustrate the theoretical findings using a non-standard finite difference (NSFD) scheme. In contrast, Muhammad F. et al. [21] propose a more sophisticated model for studying the behavior of Hepatitis B in a population. Ahmad et al. [1] introduced a deterministic SEIR-based model to analyze Ebola disease. They employed optimal control strategies for hospitalization (with and without quarantine) and vaccination to forecast potential future outcomes regarding resource utilization for disease control and the effectiveness of vaccination in affected populations. Ahmad et al. [2] highlight that, despite advancements in vaccination programs, measles outbreaks continue to occur. The authors introduce a deterministic SVEITR model to describe the disease dynamics and conduct an in-depth analysis of the model's behavior. Additionally, they formulate an optimal control problem aimed at reducing infectivity within the population. Felix K. et al. [35] introduce a novel approach to deterministic modeling of the Covid-19 epidemic using an integro-differential equation. They demonstrate that the proposed model shares similarities with classic compartmental models like SIR. A key advantage of this approach is that the model's dynamics are described using a single equation. Charpentier et al. [13] proposed a Covid-19 model that implicitly accounts for undetected infected individuals. The author formulated an optimal control problem to identify strategies that can help control the pandemic by maintaining a low level of infectious individuals.

Deterministic models are useful examples that provide important information. However, they do not capture the uncertainties involved in the randomness of disease transmission and progression. Stochastic epidemic models address this limitation by incorporating the probabilistic nature of interactions and transmissions. This allows them to offer a more realistic picture of epidemic dynamics. As a result, many disease dynamics have been studied from a stochastic perspective. This has enhanced the realism and accuracy of the analysis.

**Literature review on Stochastic Epidemic Model.** The formulation of stochastic models can be undertaken in various ways. Linda J.S. Allen, in her work [4], presents different approaches to formulating stochastic models. She discusses three primary methods: discrete time Markov chains, continuous time Markov chains, and stochastic differential equations. Furthermore, she explores valuable properties for analyzing stochastic epidemiological models, such as the probability of disease extinction and the probability of disease outbreak [5].

In [6], Linda J.S. Allen and Glenn E.L. propose a stochastic multigroup model based on continuous-time Markov chains (CTMC) to address the issue of disease extinction. A few years later, Linda J.S. Allen and Xueying Wang developed a stochastic model for cholera using branching process theory to analyze the probability of disease extinction [7]. The author Diderot X. et al [17] proposed a new stochastic model describing the course of bubonic plague epidemics in rat and human populations. In their modeling, they considered rat and human populations separately, providing a better understanding of the dynamics of bubonic plague in both populations. Moiz et al. [48] propose a stochastic model combining the Auto-Regressive Integrated Moving Average (ARIMA) methodology with a Neural Networks approach to predict the global cumulative cases of "monkeypox virus" (MVP) at peak levels. Bärbel F. et al. [23] proposed a stochastic model to explain extinction and

recurrence of epidemics observed in measles. Bing G. et al. [28] presents a detailed investigation of a stochastic model based on the SEIR framework with vaccination. This model governs the spread of the measles virus while incorporating white noise and the effects of immunizations. The latest pandemic of Covid-19 has been the focus of much attention from researchers, who have proposed numerous studies to understand the evolution of the disease [10],[41], [9], [51] and how to control it [32],[19], [39]. The Covid-19 pandemic emphasized the critical role of such models in predicting the spread of infectious diseases and supporting public health decisions. Accurate modeling has become increasingly important to guide interventions and mitigate the impact of outbreaks.

Traditional epidemic models, such as the SIR model and SEIR model are often limited by their assumption of complete knowledge about the state of the epidemic, which is not realistic in the face of incomplete or noisy data and also when we are using a model like SEIR with a compartment E denoting individuals exposed to the disease, but not yet infectious. Particularly, unobserved cases, such as asymptomatic individuals and delays in testing, contribute to the significant challenges in accurately estimating the current state of an epidemic [53], [15] and the key model parameters [31], [50]. Stochastic epidemic models offer a flexible alternative, allowing the incorporation of randomness and uncertainty in epidemic dynamics.

**Our Contribution.** This study develops a sophisticated stochastic model for Covid-19, taking into account the partially observable states. The model dynamics incorporate cascade states to capture as much relevant information as possible, thereby enhancing model accuracy. In the context of Covid-19, these cascade states allow us to account for the gradually fading immunity from vaccination and recovery, as neither provides complete immunity.

The model is primarily constructed based on the concept of chemical reaction networks as detailed in [8] and [12]. We applied an CTMC framework and derived a diffusion approximation using the law of large numbers and the central limit theorem for Poisson processes.

The inclusion of cascade states is motivated by the fact that, in models with hidden compartments, it is possible for these compartments to have one or more observable incoming transitions while at least one outgoing transition remains unobservable (or vice versa). To leverage the information from observed incoming transitions, the compartment can be divided into a series of generic sub-compartments, each of them grouping individuals based the time elapsed since they first entered the compartment.

The proposed model enables the application of filtering techniques for parameter or state estimation. The numerical results for the proposed Covid-19 model are designed with flexibility to account for time-varying parameters, which have been estimated based on both the developed model and real data from the Robert Koch-Institute (RKI) in Germany. Finally, we present the results of numerical experiments showing the evolution in each compartment. The dynamics obtained from our proposed model, particularly for the infected individuals, closely resemble the observations in Germany during the pandemic

**Paper Organization.** In Section 2, we begin with the mathematical foundation of the proposed model, starting with the microscopic model based on CTMC. Later, in Section 3, we present some limit properties which lead to the diffusion approximation. In Section 4, we provide model examples, particularly focusing on the Covid-19 model. This section also

motivates the introduction of the cascade state and concludes with the Covid-19 model with the cascade state. Section 5 primarily discusses the model parameter estimation method, where we used ridge regression for parameter estimation. In Section 6, we present the numerical experiments: first, for the time-dependent model estimation, and second, for the proposed Covid-19 model with the cascade state.

## 2 Microscopic Models

Let  $(\Omega, \mathcal{F}, \{\mathcal{F}_t\}_{t \geq 0}, \mathbb{P})$  be a filtered probability space and  $X = (X(t))_{[0, T]}$ , a stochastic process which takes values in  $\{0, \dots, N\}^d$  in a fixed time interval  $[0, T]$ . The  $\sigma$ -algebra  $\mathcal{F}_t$  model the information about the system from observing  $X$  that is available at time  $t$ . Here  $X_i(t) \in \{0, \dots, N\}$  denotes the absolute size of subpopulation in compartment  $i = 1, \dots, d$  at time  $t \geq 0$ . We denote by  $\bar{X}_i = \frac{1}{N}X_i \in [0, 1]$  the relative size of subpopulation in compartment  $i = 1, \dots, d$ . As our aim is to study changes in the number of individuals in each compartment over time, we will focus mainly on the absolute size of subpopulations.

### 2.1 Counting processes

Let us denote by  $M_k(t)$  the total number of transition  $k = 1, \dots, K$  in the time interval  $[0, t]$ . Since each transition corresponds to an individual moving from one compartment to another,  $M_k(t)$  represents the total number of such transitions (or individuals) of type  $k$  that occur within the time interval  $[0, t]$ ,  $k \in \{1, \dots, K\}$ . For all  $k \in \{1, \dots, K\}$ ,  $M_k(t)$  can be naturally consider as counting process. In fact, for all  $k \in \{1, \dots, K\}$  and for all  $t \in [0, T]$ ,  $M_k(t) \geq 0$ . In particular for  $t = 0$ ,  $M_k(0) = 0$ . The total number of transition is non-decreasing such that for  $s \leq t$  we have  $M_k(s) \leq M_k(t)$ . Finally, the increment  $M_k(t) - M_k(s)$  equals the number of transition  $k$  that have occurred in the time interval  $[s, t]$ .

Now we can characterize the dynamic of  $X$  in term of  $M_k$  for all  $t \geq 0$ .

For a given compartment, each random transition that takes place leads to either an individual leaving the compartment or entering it, except when that compartment is not part of the transition. Therefore, for each process  $X_i(t)$ ,  $i = 1, \dots, d$ , at a given time  $t$  such that  $X_i(t) \in \mathbb{N}$ , a transition  $k$  is always of the form  $X_i(t + \Delta t) = X_i(t) + \xi_k^i$  where

$$\xi_k^i = \begin{cases} -1 & \text{if an individual leaves compartment } i \\ +1 & \text{if an individual enters compartment } i \\ 0 & \text{otherwise} \end{cases}$$

Consequently, the process  $X(t)$  is stochastic such that  $X(t) \in \mathbb{N}^d$  and

$$X(t) = X(0) + \sum_{k=1}^K \xi_k M_k(t) \text{ where } \xi_k \text{ is a } d\text{-dimensional vector constituted by } 0, 1 \text{ and } -1.$$

In the context of an epidemic model, we assume that transitions between compartments are independent of each other. To incorporate a more general perspective, we will introduce temporal variability into some of the model's key parameters, allowing greater flexibility and adaptability to reflect dynamic changes over time. This generalization aligns with realism in epidemic models, as factors like infection rates may fluctuate over time due to disease mutations, as noted in ([15],[31]). One of the most important type of counting process is the Poisson process. In this work we are going to consider the non-homogeneous Poisson process with continuous rate function  $\lambda_k(t, x)$ ,  $\forall t \geq 0$  and  $k = 1, \dots, K$ .

**Remark 2.1** Considering a homogeneous Poisson process, particularly with a constant intensity rate, is crucial when analyzing the early stages of an epidemic using an epidemic model. During this phase, the epidemic's dynamics are relatively stable, and the model parameters can reasonably be assumed to remain constant. This simplifies the mathematical framework, making the homogeneous Poisson process a valuable tool for studying and understanding the spread of the epidemic under these conditions.

Let us denote by  $\tau_k(t) = \int_0^t \lambda_k(s, X(s)) ds$  the cumulative rate function also known as the time change. Then the number of transition  $k$ , in any time interval  $[0, t]$  is Poisson distributed with mean  $\tau_k(t)$ , with respect to the transition  $k$ . By considering the number of arrival in some very small interval  $(t, t + \Delta t]$ , we obtain that  $\mathbb{P}[M_k(t + \Delta t) - M_k(t) = 0] = 1 - \lambda_k(t, X(t))\Delta t + o(\Delta t)$ ,  $\mathbb{P}[M_k(t + \Delta t) - M_k(t) = 1] = \lambda_k(t, X(t))\Delta t + o(\Delta t)$  and  $\mathbb{P}[M_k(t + \Delta t) - M_k(t) \geq 2] = o(\Delta t)$ . Now let  $\lambda_1(t, x), \dots, \lambda_K(t, x)$  be the rate function such that  $\sum_{k=1}^K \lambda_k(t, x) = \Lambda(t, x) > 0$ . Any transition from a given state  $x$  of a given rate  $\Lambda(t, x)$  Poisson process is classified as a type  $k$  transition with probability  $\frac{\lambda_k(t, x)}{\Lambda(t, x)}$  when occurring at time  $t$ . Let  $(M_k(t))_{t \geq 0}$  be the resulting counting process of type  $k$  transition for  $k = 1, \dots, K$ . In this study, the counting processes  $(M_1(t))_{t \geq 0}, \dots, (M_K(t))_{t \geq 0}$  are considered to be independent non-homogeneous Poisson processes with rate function  $\lambda_1(t, x), \dots, \lambda_K(t, x)$  respectively. In fact, the number of transitions up to  $t$  is independent because  $\forall k \in \{1, \dots, K\}$  each counting process  $M_k(t)$  does not influence others in the whole time horizon. For example, in the context of a General epidemic model, transitions such as infection have no impact on recovery or loss of immunity. Now, let us denote by  $Y_k(\cdot)$ , some independent standard Poisson processes with unit intensity and consider the defined time change  $\tau_k(t) = \int_0^t \lambda_k(s, X(s)) ds$ . The non-homogeneous Poisson processes  $M_k$  can be expressed in terms of  $Y_k(\cdot)$  as follows  $M_k(t) = Y_k(\tau_k(t))$  and the state dynamics takes the following form

$$X(t) = X(0) + \sum_{k=1}^K \xi_k Y_k \left( \int_0^t \lambda_k(s, X(s)) ds \right) \quad (2.1)$$

$(X(t))_{t \geq 0}$  is a stochastic process that evolves through a discrete set of states  $\{0, \dots, N\}^d$  over continuous time, where the system's future state depends only on its current state. The Markov process  $X(t)$  has the transition rate  $\lambda_k(t, x)$  such that

$$\mathbb{P}[X(t + \Delta t) - X(t) = \xi_k | X(t)] = \mathbb{P}[M_k(t + \Delta t) - M_k(t) = 1] \approx \lambda_k(t, X(t)) \Delta t$$

Thus,  $X$  is a non-homogeneous continuous-time Markov chain (CTMC) ([8],[12]) which takes values in  $\{0, \dots, N\}^d$ . The dynamics of the CTMC can be characterized by analyzing both the timing of the chain's transitions and the specific states to which it moves. In the context of simulation algorithms for epidemic dynamics, the classical representation involving the transition rate  $\lambda_k(t, X(t))$  aligns closely with Gillespie's algorithm [26].

## 2.2 Adapted Gillespie Algorithm for CTMC Simulation

Now we consider  $M_k(t)$ ,  $k = 1, \dots, K$  which gives the number of transition  $k$  that has been occurred during the window of time  $[0, t]$ . For  $t, s \geq 0$  ( $s \leq t$ ), for  $k = 1, \dots, K$  we have  $M_k(t) - M_k(s) \sim Poi \left( \int_s^t \lambda_k(u, X(u)) du \right)$ . We consider  $\bar{\tau}_k$  the random waiting time with respect to transition  $k$ .

We introduce  $h \geq 0$  which verified  $h \leq \bar{\tau}_k$  and assume that the process  $X(t)$  remains the same between instants  $t$  and  $t+h$ . This means that  $X(t)$  is constant during the waiting time before the transition. Because of that we will stress only the fact that we will consider later that  $\lambda_k(t, x(t)) = \lambda_k(t)$ . However, for any infinitesimally small quantity  $\delta h$ , a jump takes place between instants  $t+h$  and  $t+h+\delta h$ . We assume that  $M_k(t)$  is known, then the probability that the waiting time  $\bar{\tau}_k$  is greater than  $h$  knowing  $M_k(t)$  is the conditional survival function of  $h$  which takes the following form

$$\mathbb{P}[\bar{\tau}_k > h | M_k(t)] = \mathbb{P}[M_k(t+h) - M_k(t) = 0 | M_k(t)] = \exp \left[ - \int_t^{t+h} \lambda_k(u, x(u)) du \right] = \bar{F}_{k,t}(h)$$

The conditional density can derive trough the relation between the survival function and the density given by  $f_{k,t}(h) = -\frac{\partial}{\partial h} \bar{F}_{k,t}(h)$ . And based on the Leibniz integral rule we obtain

$$f_{k,t}(h) = \lambda_k(t+h) \exp \left[ - \int_t^{t+h} \lambda_k(u, x(u)) du \right]$$

Using the density function and the survival function we can compute the hazard rate

$$\lambda_k(t+h) = \frac{f_{k,t}(h)}{\bar{F}_{k,t}(h)}$$

which characterizes the probability of transition in an infinitesimal period of time after  $t+h$ , conditional on the absence of transition before  $t+h$ . Now we introduce  $\bar{\tau}$  the waiting time until the next transition (of any type ) occurs

$$\bar{\tau} = \bar{\tau}_1 \wedge \bar{\tau}_2 \wedge \dots \wedge \bar{\tau}_n$$

Since all the counting process  $M_k(t)$ ,  $k = 1, \dots, K$  are independents then

$$\{\bar{\tau} > h\} = \{\bar{\tau}_1 > h\} \cap \{\bar{\tau}_2 > h\} \cap \dots \cap \{\bar{\tau}_K > h\}$$

the survival function with respect to  $h$  can be compute as follows

$$\bar{F}_t(h) = 1 - F_t(h) = \mathbb{P}(\{\bar{\tau} > h\}) = \prod_{k=1}^K \mathbb{P}(\{\bar{\tau}_k > h\}) = \exp \left[ - \int_t^{t+h} \sum_{k=1}^K \lambda_k(u) du \right]$$

Let us denote  $\Lambda(t) = \sum_{k=1}^K \lambda_k(t)$ , then the above integral can be written in the following way

$$\bar{F}_t(h) = \exp \left[ - \int_t^{t+h} \Lambda(u) du \right] = \exp \left[ - \int_0^h \Lambda(t+u) du \right]$$

Now knowing the expression of the survival function  $\bar{F}_t(h)$ , we can simulate the waiting time  $\bar{\tau}$  by using the inverse method (or quantile transformation). We draw  $\xi$  uniformly in the interval  $(0, 1)$  and solve the equation  $\xi = \bar{F}_t(h)$  which is equivalent to

$$\log(\xi) = - \int_0^h \Lambda(t+u) du$$



For  $\Lambda(t)$  constant, and verify  $\Lambda(t) = \Lambda_0$ , the waiting time  $\bar{\tau} = -\frac{\log(\xi)}{\Lambda_0}$ . This outcome aligns with what is achieved in the conventional Gillespie algorithm.

For  $\Lambda(t)$  slowly varying, then we can approximate the integral  $\int_0^h \Lambda(u+t)du$  by  $h\Lambda(t)$  and derive an approximation of the waiting time  $\bar{\tau} = -\frac{\log \xi}{\Lambda(t)}$ .

For an exact solution, let introduce  $B_t(h) = \int_0^h \Lambda(t+u)du$ . We know that the waiting time is obtain by solving the equation

$$B_t(h) + \log(\xi) = 0$$

Most of case  $B_t(h)$  is unknown explicitly or the form of  $\Lambda(t)$  is complex and then make difficult to find an exact solution of the above equation. One solution is to use an approximation method to solve the corresponding non-linear equation. As an illustration, employing the Newton-Raphson method allows one to estimate the solution of the equation above in the following manner:

$$\bar{\tau}_{n+1} = \bar{\tau}_n - \frac{B_t(\bar{\tau}_n) + \log(\xi)}{B'_t(\bar{\tau}_n)}, \quad \bar{\tau}_0 = -\frac{\log(\xi)}{\Lambda(t_0)}$$

Now we know how to estimate the waiting  $\bar{\tau}$  in the case where the intensity rate is constant or time-dependent. The next step is to be able to determine which transition among all the  $k, k \in \{1, \dots, K\}$  transitions will take place. The transition probabilities of the embedded Markov chain  $(X_n)$  are, for  $\xi_k, k = 1 \dots, K, \{\xi_1, \dots, \xi_K\}$  is given as follow

$$\mathbb{P}[X_{n+1} = x + \xi_k | X_n = x] = \frac{\lambda_k(n, x)}{\sum_k \lambda_k(n, x)}$$

Following the transition, we move from state  $x$  to  $x'$ . The sampling of the arrived state  $x'$  is based on a specific transition vector  $x' = x + \xi_{k^*}$ . The simulation of the choice  $k^* \in \{1, \dots, K\}$  can be achieved by using the cumulative sum approach. This approach can be describes as follows: compute the sum  $p_{k^*} = \sum_{k=1}^{k^*} \frac{\lambda_k(t + \bar{\tau})}{\Lambda(t + \bar{\tau})}$  and draw uniformly a random number  $r$  in a such away that  $k^*$  verify  $p_{k^*-1} \leq r < p_{k^*}$ .

### 3 Macroscopic Model

In this section, we explore the link between stochastic models, characterized by continuous-time Markov chains, and models based on ordinary differential equations (ODEs). In addition, we perform a comparative analysis between deterministic and stochastic frameworks to stress their advantages and limitations in the field of epidemic modeling. More specifically, with regard to sub-population size, we will take advantage of the law of large numbers for Poisson processes to demonstrate that as we increase the total population size  $N$ , the CTMC converges to a deterministic limit.

**Algorithm 2.1** Simulation of Non-Homogeneous CTMC

---

**Data:**  $X_0, \xi_k, k := 1, \dots, K, T$   
**Input:**  $\theta_1(t), \dots, \theta_m(t)$  // Model parameters  
**Output:**  $X := \{X(t), t \in [0, T]\}$   
**Initialization :**  $t := 0 ; X(t) := X_0$   
**while**  $t < T$  **do**  
    Draw  $\xi$  with standard uniform distribution  
    Solve  $B_t(h) + \log(\xi) = 0$  and obtain  $\bar{\tau}$  // Simulate the Waiting Time  
    // Determine the Next Transition  
    **for**  $k := 1$  **to**  $K$  **do**  
         $p_k := \sum_{i=1}^k \frac{\lambda_k(t + \bar{\tau})}{\Lambda(t + \bar{\tau})}$   
    **end**  
    Draw  $r$  with standard uniform distribution  
    Pick  $k \in \{1, \dots, K\}$  such that  $p_{k-1} \leq r < p_k$   
    // Update the state and time dynamic  
     $X(t + \tau) := X(t) + \xi_k$   $t := t + \bar{\tau}$   
**end**

---

**3.1 Law of Large Numbers and ODE Models**

We consider a constant population size  $N$ . Let us recall the state dynamic  $X(t)$  driven by the CTMC and which the form is as follow :

$$X(t) = X(0) + \sum_{k=1}^K \xi_k Y_k \left( \int_0^t \lambda_k(s, X(s)) ds \right) \quad k = 1, \dots, K.$$

Here,  $Y_k$  denotes a set of mutually independent standard Poisson processes, each operating at a unit rate. The function  $\lambda_k(t, X(t))$  represents the jump rate corresponding to the transition  $\xi_k$  at time  $t$ . The transition vector  $\xi_k$  is a  $d$ -dimensional vector, typically taking values within the set  $\mathbb{N}^d$ . The  $i$ -th component of the  $X(t)$  vector represents the population size in the  $i$ -th compartment at time  $t$ . Notably, this dynamic can also be expressed in terms of relative sub-population sizes, where we define  $\bar{X}^N(t)$  as the vector obtained by scaling  $X(t)$  by  $1/N$  such that  $\bar{X}^N(t) = \frac{1}{N} \times X(t)$ . Given the context of a constant population size ( $N(t) = N$ ), the components of  $\bar{X}^N(t)$  represent the proportions of the total population within various compartments at time  $t$ .

The equivalent equation for  $\bar{X}^N(t)$  can be written in the following way :

$$\bar{X}^N(t) = \bar{X}^N(0) + \sum_{k=1}^K \frac{1}{N} \xi_k Y_k \left( \int_0^t \lambda_k(s, N\bar{X}^N(s)) ds \right) \quad k = 1, \dots, K$$

We assume that there exist a collection of function  $v_k(.,.) : \mathbb{R}^+ \times [0, 1]^d \rightarrow \mathbb{R}^+$  such that

$$(H1) \quad \forall k \in \{1, \dots, K\}, \quad v_k(.,.) \in C^2([0, T] \times [0, 1]^d)$$

$$(H2) \quad \forall k \in \{1, \dots, K\}, \quad x \in [0, 1]^d, t \in [0, T] \quad \frac{1}{N} \lambda_k(t, \lfloor Nx \rfloor) \longrightarrow v_k(t, x) \quad \text{as } N \longrightarrow \infty$$

where  $\lfloor Nx \rfloor$  is a vector of integers.

**Remark 3.1** Typically, within the context of epidemic models, the following relationship holds true for each transition:  $\lambda_k(t, \lfloor Nx \rfloor) = Nv_k(t, x)$  for all  $k = 1, \dots, K$ ,  $N \geq 1, x \in [0, 1]^d$  and  $t \in [0, T]$  (See [12]). In particular, this relation is fulfill when the intensity rate  $\lambda_k(t, x)$  is linear or quadratic of the form  $\frac{xy}{N}$  with  $x, y \in \{0, \dots, N\}^d$ .

Based on the above remark we can rewrite  $\bar{X}^N(t)$  as

$$\bar{X}^N(t) = \bar{X}^N(0) + \sum_{k=1}^K \frac{1}{N} \xi_k Y_k \left( \int_0^t Nv_k(s, \bar{X}^N(s)) ds \right) \quad k = 1, \dots, K$$

Therefore,  $\bar{X}^N$  shows a behavior close to  $X$ , but the magnitudes of its jumps are scaled by a factor of  $1/N$ . Consequently, with an increase in  $N$ , the jumps of  $\bar{X}^N$  diminish in size. Intuitively, as  $N$  becomes large,  $\bar{X}^N$  may approach a potentially continuous limit. In this context of a large  $N$ , the mathematical exploration of the limit of  $\bar{X}^N$  has been primarily undertaken by Kurtz [[36], [37], [38]]. These works consider a time-independent intensity. Then, Guy [[29],[30]] and Nacir et al. ([45]) have obtained more generalized results on convergence and diffusion approximation, accounting for time-dependent intensities in all Poisson processes considered.

In the subsequent discussion, we assume that the intensity rates  $v_k$  are locally bounded, a property typically met within the framework of epidemic models with constant total population size. We know that  $Y_k(t)$  is a standard Poisson process, then  $\tilde{Y}_k(t)$  defined by  $\tilde{Y}_k(t) = Y_k(t) - t$ ,  $k = 1, \dots, K$  are continuous time martingales as defined in the appendix of [12]. Based on that, we can rewrite the dynamic of  $\bar{X}^N$  and obtain

$$\bar{X}^N(t) = \bar{X}^N(0) + \int_0^t \bar{F}(s, \bar{X}^N(s)) ds + \sum_{k=1}^K \frac{1}{N} \xi_k \tilde{Y}_k \left( \int_0^t Nv_k(s, \bar{X}^N(s)) ds \right) \quad k = 1, \dots, K$$

where  $\bar{F}(t, x) = \sum_{k=1}^K v_k(t, x) \xi_k$ .

**Theorem 3.2 (Law of Large Numbers)** *Assume that the initial condition  $x_0 \in [0, 1]^d$  is given such that  $\bar{X}^N(0) \rightarrow x_0$  as  $N \rightarrow \infty$ . In addition based on (H2),  $\bar{F}(t, x) = \sum_{k=1}^K v_k(t, x) \xi_k$  is locally Lipschitz as a function of  $x$ , and locally uniformly<sup>1</sup> in  $t$ , then  $\bar{X}^N(t)$  converges almost surely uniformly on  $[0, T]$  to the solution  $\bar{X}^\infty(t)$  of the ordinary differential equation (ODE)*

$$\frac{d\bar{X}^\infty(t)}{dt} = \bar{F}(t, \bar{X}^\infty(t)); \quad \bar{X}^\infty(0) = x_0$$

*Proof.* The proof of this theorem is mainly based on the above proposition and Gronwall's Lemma. All the details can be found in [12]

<sup>1</sup> The "locally uniformly" in  $t$  ensures that the Lipschitz constant does not vary excessively  $t$  changes within a bounded region.

### 3.2 Central Limit Theorem

In the framework of stochastic epidemic model, it is recognized that diffusion processes provide a reliable approximation for describing the dynamics within each sub-compartment (Guy et al., [29]). In this section, we explore variations in the disparity between the stochastic epidemic process and its deterministic limit.

Let us define  $G(t)$  as the scale deviation between  $\bar{X}^N(t)$ , representing the stochastic process describing changes in the proportions of the total population in the different compartments, and its deterministic limit  $\bar{X}^\infty(t)$ .

$$G^N(t) = \sqrt{N} \left( \bar{X}^N(t) - \bar{X}^\infty(t) \right) \quad (3.5)$$

Based on [[12],[29],[30]],  $G^N(t) \rightarrow G(t)$  as  $N \rightarrow \infty$  is centered Gaussian process and has the form

$$G^N(t) = G^N(0) + \sqrt{N} \int_0^t \left[ F(X^N(s)) - \bar{F}(\bar{X}^\infty(s)) \right] ds + \sum_{k=1}^K \xi_k \tilde{\mathcal{N}}_k^N(t)$$

where  $G^N(0) = \sqrt{N} \left( X^N(0) - \bar{X}^\infty(0) \right)$ ,  $\tilde{\mathcal{N}}_k^N(t) = \frac{1}{\sqrt{N}} M_k \left( N \int_0^t \mathbf{v}_k(X^N(s)) ds \right)$

The following result is very important in the stochastic process approximation procedure.

**Proposition 3.3** *As  $N \rightarrow \infty$   $\{ \tilde{\mathcal{N}}^N(t), t \geq 0 \}$  convergence in distribution to  $\{ \tilde{\mathcal{N}}(t), t \geq 0 \}$ , where  $\tilde{\mathcal{N}}^N(t) = \int_0^t \sqrt{\mathbf{v}_k(s, \bar{X}^N(s))} dW_k(s)$  and  $W_1(t), \dots, W_k(t)$  are mutually independent standard Brownian motions.*

*Proof.* The proof of this proposition is mainly based the central limit theorem for Poisson process given in the book [[12], Chapter 2].

In the following we have the main result of this section which is indeed the consequence of the above proposition ([12]),

**Theorem 3.4 (Central Limit Theorem)** *Let us assume in addition to the Theorem 3.1 that  $\bar{F}(x)$  is of class  $\mathcal{C}^1$ , locally uniformly in  $t$ . Then  $\forall t \geq 0$ ,  $G^N(t) \xrightarrow[N \rightarrow +\infty]{} G(t)$*

where

$$G(t) = \int_0^t \nabla \bar{F}(s, \bar{X}^N(s)) G(s) ds + \sum_{k=1}^K \xi_k \int_0^t \sqrt{\mathbf{v}_k(s, \bar{X}^N(s))} dW_k(s), \quad t \geq 0$$

*Proof.* For all details about the proof of this main result one can refers to [12] and [8].

### 3.3 Numerical Illustration of Limit Theorems

This section focuses on the numerical simulation study of a SIRS model, 3.1. The subsection addresses the simulation of a CTMC model using the classic SIRS framework,

followed by a numerical demonstration of the law of large numbers and the central limit theorem using this model.

For the simulations, we will consider a time-dependent infection rate  $\beta(t) = \beta_0(1 + A \sin(\frac{2\pi t}{T^\beta}))$  where  $\beta_0$  is the baseline infection rate,  $A$ , the amplitude of the seasonal effect,  $T^\beta$  the period of the seasonal trend on transmission and finally  $t$ , the time (Ex: in days, weeks,..etc.). The recovery rate  $\gamma$  and the losing immunity  $\rho$  are set respectively as  $\gamma = \rho = 0.05$  and  $\beta_0 = 0.2$ ,  $A = 0.4$  and  $T^\beta = 365$ . According to this model (3.1), we have the following table which describes the different transition which are going to be used in the algorithm 2.1 in order to simulate the CTMC.

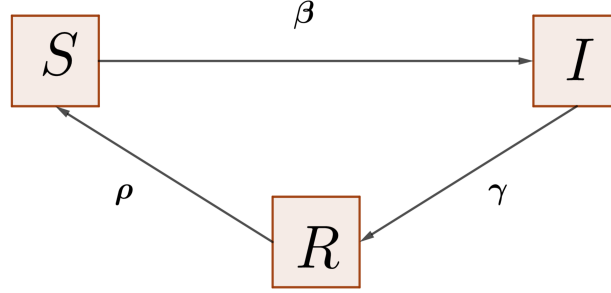


Fig. 3.1: SIRS model with different transitions

Table 3.1: SIRS model : State process  $X = (X_1, X_2, X_3) = (I, R, S)$ ; Total number of states  $d = 3$ , Total transitions  $K = 3$ .

k	Transition	Transition vectors $\xi_k$	intensity $\lambda_i(t, X)$
1	Infection of susceptible	$(1, 0, 0)^\top$	$\beta(t)S \frac{I}{N} = \beta X_1 \frac{X_2}{N}$
2	Recovering of infected non-detected	$(-1, 1, 0)^\top$	$\gamma I = \gamma X_1$
3	Losing immunity	$(0, -1, 1)^\top$	$\rho R = \rho X_2$

Based on the algorithm 2.1, we can visualize the paths of this SIRS model as given in the Figure 3.2. We should note that in Figure 3.2, a small sample size ( $N = 10$ ) was used to clearly illustrate the different jumps that occur over time. Now, focusing on the infected compartment, we consider  $\bar{I}(t)$  as the solution of the deterministic model associated with the SIRS model, based on Theorem 3.2. For demonstrating the Law of Large Numbers, we will now examine five different population sizes. This will show that as the population size increases, the model, which was initially described by a CTMC chain, will gradually "converge" towards deterministic behavior. In other words, the model's output will appear progressively smoother as the population size grows larger. Formally, we simulate 10 sample paths for the CTMC SIRS model. By progressively increasing the total population size  $N$ , we observe that the paths of  $I^N(t)$  converge toward the deterministic counterpart  $\bar{I}(t)$ .

The concept of the CLT becomes relevant when examining deviations around the ODE limit based on the corresponding CTMC model. For illustration, we consider the Gaussian

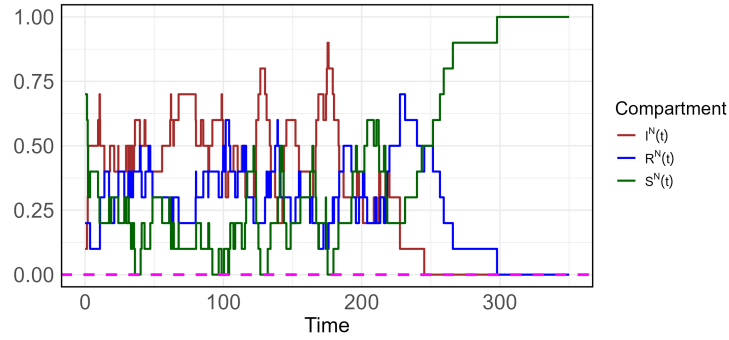
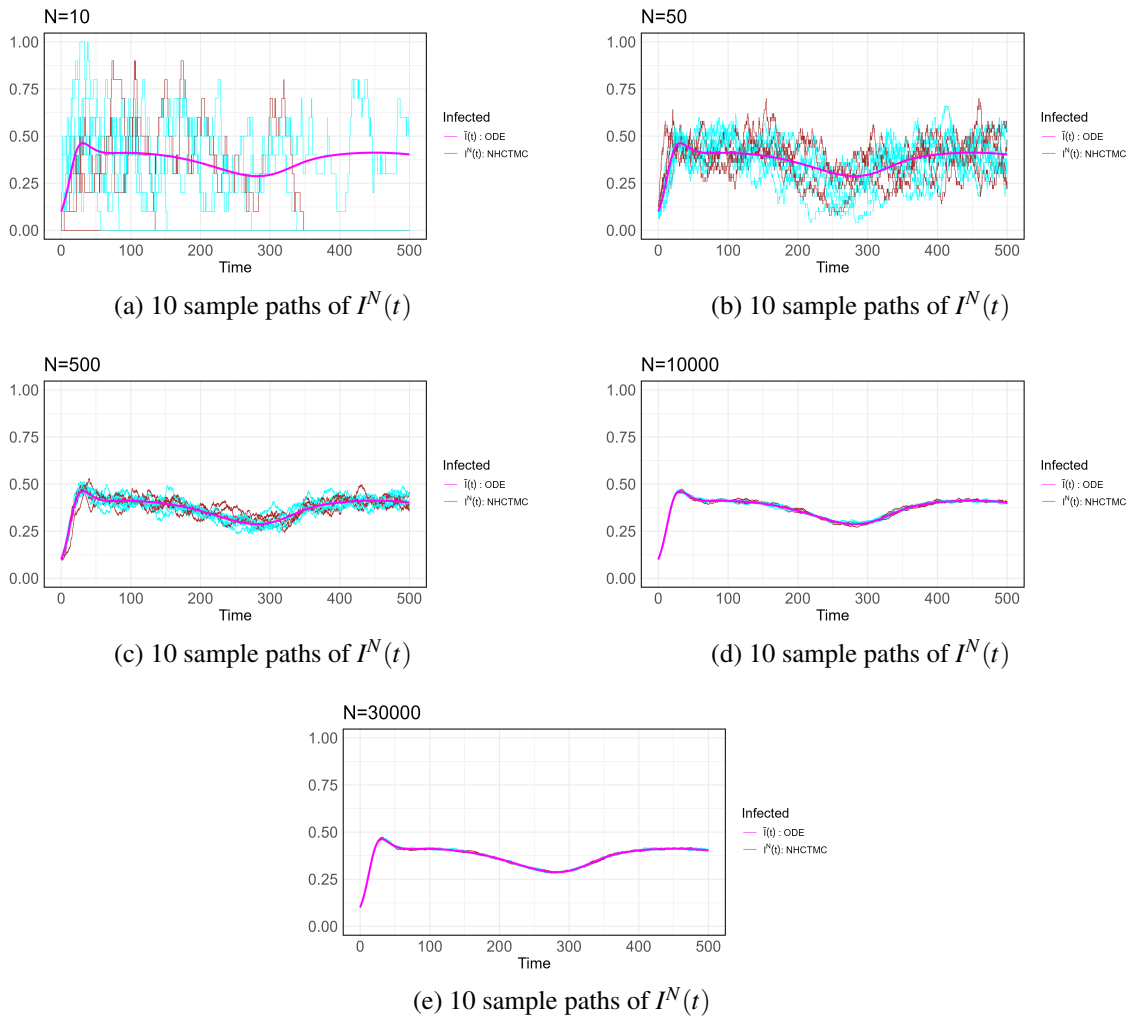
Fig. 3.2: NHCTMC SIRS model Simulation,  $N=10$ 

Fig. 3.3: Illustration of the Law of Large Numbers (LLN) using the SIRS model: as the population size  $N$  increases, all paths from CTMC becomes progressively smoother and converge to  $\bar{I}(t)$ .

process defined by Equation (3.5). Using the CTMC SIRS model, we simulate 10 sample paths for  $I^N$  and compute the quantity  $\sqrt{N}(I^N - \bar{I}(t))$ . As the population size increases, we

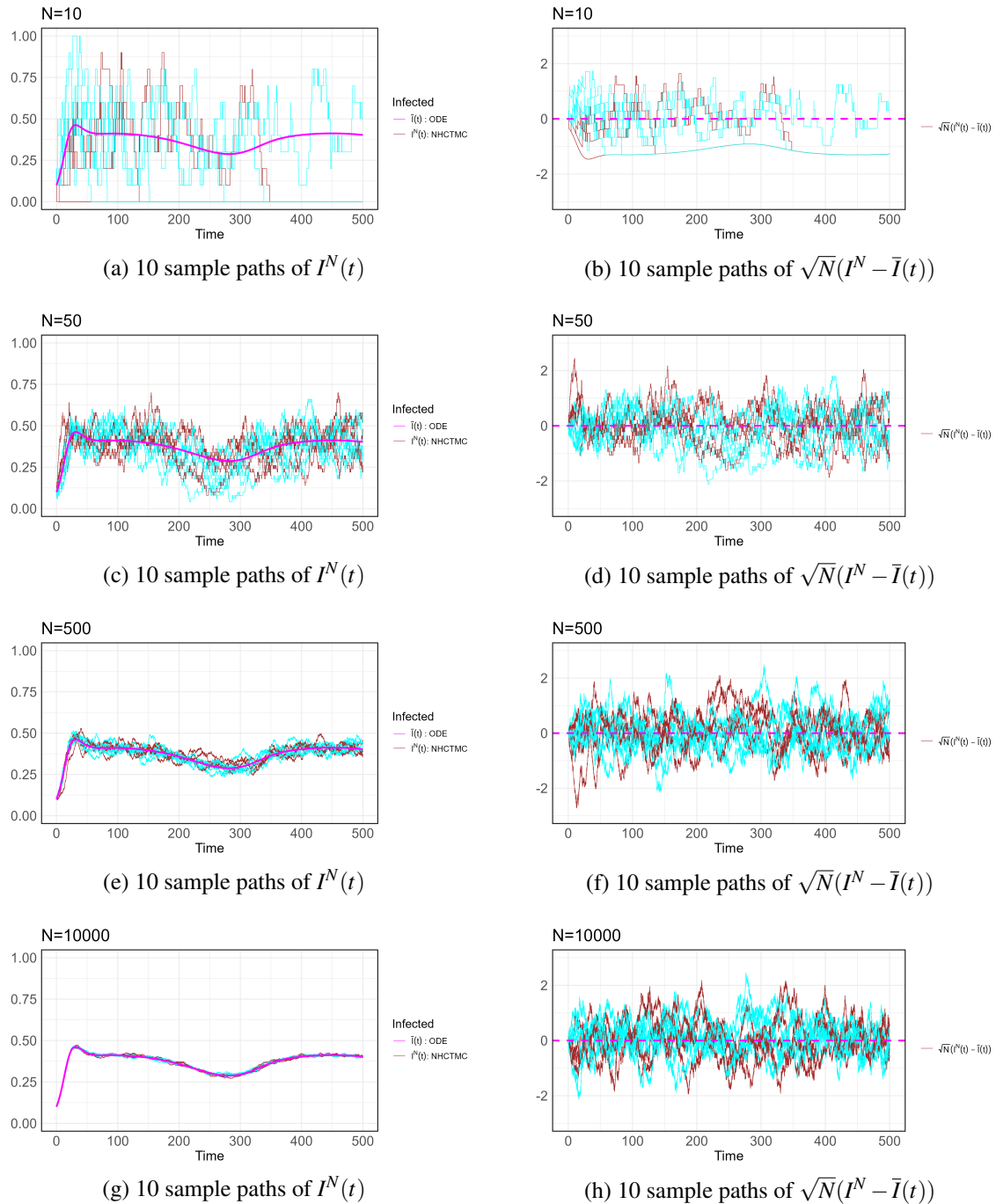


Fig. 3.4: Illustration of the Central Limit Theorem (CLT) using the SIRS model: as the population size  $N$  increases, all paths from CTMC starting from zero always deviate to 0.

observe the convergence of the CTMC model to the deterministic model. Simultaneously, the variable defined by (3.5) ( $\sqrt{N}(I^N - \bar{I}(t))$ ) according to the process  $I^N$  involved in the model, starting from 0, consistently fluctuates around 0.

### 3.4 Diffusion Approximation

The construction of the diffusion process as an approximation of the multidimensional model, driven by continuous-time Markov chains, depends on whether the model parameters (intensities rate) depend on time or not. In the case of homogeneous CTMCs, the construction of the approximation via a diffusion process has been studied by Britton and Pardoux [12], Anderson and Kurtz [8], as well as Ethier and Kurtz ([20], chapter 4, section 7). However, these authors examined diffusion approximations of jump processes only in the case of time-homogeneous transition rates. To account for time dependence in the approximation, Guy et al. (2015, [29]) relied on the work of Ethier and Kurtz, but using a different technique as their time change Poisson processes representation to demonstrate the central limit theorem. In addition, they demonstrated that the jump process and the diffusion both converge to the same Gaussian process. In their generalization, they include systems that are non-homogeneous in time, thus allowing the treatment of complex epidemic models, especially those dependent on time (see Appendix A3. [29]).

Now we recall the multi-dimensional CTMC describing in one hand the dynamic of the absolute sub-population size in each compartment,  $X(t)$  and the other hand the dynamic of the relative sub-population size in each compartment,  $\bar{X}^N(t)$ .

$$X(t) = X(0) + \sum_{k=1}^K \xi_k Y_k \left( \int_0^t \lambda_k(s, X(s)) ds \right) \quad k = 1, \dots, K$$

$$\bar{X}^N(t) = \bar{X}^N(0) + \sum_{k=1}^K \frac{1}{N} \xi_k Y_k \left( \int_0^t N v_k(s, \bar{X}^N(s)) ds \right) \quad k = 1, \dots, K$$

Now based on the above mentioned additional assumption [[29],[30]] we obtain the following diffusion approximations

$$d\bar{X}^D(t) = \bar{F}(t, \bar{X}^D(t))dt + \frac{1}{\sqrt{N}} \bar{\sigma}(t, \bar{X}^D(t))dW(t), \quad \bar{X}^D(0) = \bar{X}^N(0) = \bar{x}_0$$

The drift coefficient is given by  $\bar{F}(\bar{X}^N) = \sum_{k=1}^K \xi_k v_k(\bar{X}^N)$ , and the diffusion coefficient  $\bar{\sigma}(\bar{X}^N) = (\xi_1 \sqrt{v_1(\bar{X}^N)}, \dots, \xi_K \sqrt{v_K(\bar{X}^N)})$ . This diffusion approximation is based on context of relative sub-population size.

When we consider the approximation in term of absolute sub-population size we obtain

$$dX^D(t) = F(t, X^D(t))dt + \sigma(t, X^D(t))dW(t), \quad X^D(0) = X(0) = x_0 \quad (3.9)$$

with drift coefficient  $F(X^D) = \sum_{k=1}^K \xi_k \lambda_k(X^D)$ , the diffusion coefficient  $\sigma(X^D) = (\xi_1 \sqrt{\lambda_1(X^D)}, \xi_2 \sqrt{\lambda_2(X^D)}, \dots, \xi_K \sqrt{\lambda_K(X^D)})$ . In the both contexts (relative and absolute sub-population size) we have  $K$  independent standard Brownian motions  $W_1, \dots, W_K$ , such that  $W = (W_1, \dots, W_K)^T$ .

We assume that this diffusion approximation can be written as

$$dY = \bar{f}(t, Y, Z)dt + \bar{\sigma}(t, Y, Z)dW^1 + \bar{g}(t, Y, Z)dW^2 \quad (3.10)$$



$$dZ = \bar{h}(t, y, Z)dt + \bar{\ell}(t, Y, Z)dW^2 \quad (3.11)$$

We apply Euler-Maruyama time discretization to (3.10)-(3.11) by setting  $t_n = n\Delta t$ ,  $n = 0, 1, \dots, T - 1$ .

$$\begin{aligned} Y_{n+1} &= Y_n + f(n, Y_n, Z_n) + \sigma(n, Y_n, Z_n)\mathcal{E}_{n+1}^1 + g(n, Y_n, Z_n)\mathcal{E}_{n+1}^2 \\ Z_{n+1} &= Z_n + h_0(n, Y_n, Z_n) + \ell(n, Y_n, Z_n)\mathcal{E}_{n+1}^2 \end{aligned}$$

where  $(\mathcal{E}_n^1), (\mathcal{E}_n^2)$  are independent sequences of i.i.d.  $\mathcal{N}(0, \mathbb{I})$  random vectors.

## 4 Models Examples

In the following section, we introduce three important epidemic models : the measles epidemic model, the  $SI^\pm R$  model and the Covid-19 model. The measles model captures the dynamics of an infectious disease characterized by non-observed compartment, life-long immunity following recovery or vaccination. This is a classic example of the study of diseases with known modes of transmission. On the other hand, the  $SI^\pm R$  model represents a more flexible framework, incorporating both asymptomatic individuals who are not directly observed and those who are detected. This particularity of not directly observing individuals in a given compartment makes the model particularly useful for complex epidemic scenarios. Finally, Covid-19 disease presents challenges such as varying immunity duration, the presence of asymptomatic carriers, and a significant proportion of non-detected cases. In this Covid-19 model we account for these complexities, including partial immunity from infection or vaccination, and dynamic vaccination campaigns to control outbreaks. All these models will be studied to highlight their relevance in understanding disease spread and control.

### 4.1 $SI^\pm RS$ Model

We consider a stochastic SIRS epidemic model, illustrated in the Figure 4.1. In this example we assume constant total population size  $N$ . The SIRS epidemic model, consist of splitting the population into four compartments : susceptible  $S$ , infected  $I$  and recovered  $R$ ). Here,  $S$  represent the number of individuals who are susceptible to the disease, meaning they can be infected if they come into contact with an infectious person from  $I$  who is currently infected with the disease and can transmit it to susceptible people. And finally  $R$  are individuals who have recovered from the disease and developed immunity. They are no longer susceptible to contracting the disease, but they can lose their immunity and become susceptible again.

Additionally, the SIRS model can be extend to  $SI^\pm RS$  Model which allows for the differentiation between observable and hidden states of infection, aligning better with real-world scenarios. In fact, during epidemics such as Covid-19 not all cases are diagnosed. Not all infected individuals are detected, as some may be asymptomatic or refuse testing, while others test positive and are detected as infected. To account for this, we divide the compartment ( $I$ ) into two parts: one for non-detected infected individuals  $I^-$  and another for detected infected individuals  $I^+$ . The dynamics of the  $SI^\pm RS$  model (Figure 4.1 ) are governed by a set of counting processes that describe the transitions between these compartments. The main features of the model are summarized in the following table :

Table 4.1:  $SI^\pm RS$  model : State process  $X = (X_1, X_2, X_3, X_4) = (I^-, R, S, I^+)$ ; Total number of states  $d = 4$ , Total transitions  $K = 5$ .

k	Transition	Transition vectors $\xi_k$	intensity $\lambda_i(X)$
1	Infection of susceptible	$(-1, 0, 1, 0)^\top$	$\beta S \frac{I^-}{N} = \beta X_1 \frac{X_3}{N}$
2	Recovering of infected non-detected	$(-1, 1, 0, 0)^\top$	$\gamma^- I = \gamma^- X_1$
3	Recovering of infected detected	$(0, 1, 0, -1)^\top$	$\gamma^+ I^+ = \gamma^+ X_4$
4	Test of infected non-detected	$(-1, 0, 0, 1)^\top$	$\alpha I^- = \alpha X_1$
5	Losing immunity	$(0, -1, 1, 0)^\top$	$\rho R = \rho X_2$

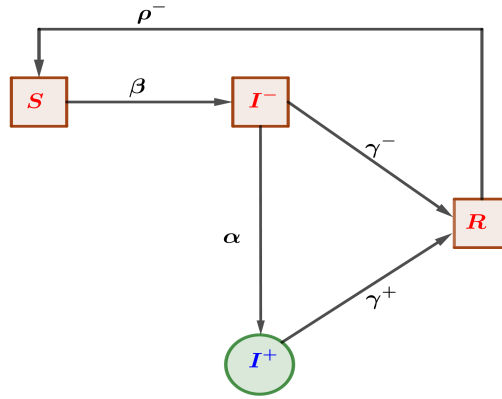


Fig. 4.1:  $SI^\pm R$  Model with different transitions

The  $SI^\pm RS$  model allows for the possibility that individuals lose their immunity over time, making them susceptible to reinfection. The dynamic of this model can be modeled using CTMC denoted as  $X(t) = (X_1(t), X_2(t), X_3(t), X_4(t))$ , where  $X_1(t) = I^-(t)$ ,  $X_2(t) = R(t)$ ,  $X_3(t) = S(t)$ ,  $X_4(t) = I^+(t)$  and  $X_1(t) + X_2(t) + X_3(t) + X_4(t) = N$ . In this model we have the total number of compartment  $d = 4$ . The model's dynamic evolution is based on five distinct possible transitions, each characterized by transition vectors  $\xi_k$ ,  $k = 1, \dots, 5$ . The changes in the sizes of each compartment are assumed to follow the dynamics described by the following SDEs. Let us recall the Figure (4.2), which illustrate the transitions of individuals from one state to another. In this case the state process is given as,  $X(t) = (Y, Z)$  with  $Y = (I^-, R, S)$  and  $Z = I^+$  and the corresponding diffusion approximation is of the form

$$dX^D(t) = F(t, X(t))dt + \sigma(t, X(t))dW(t),$$

where

$$F(t, X(t)) = \begin{pmatrix} \beta \frac{Y_1 Y_3}{N} - (\alpha + \gamma^-) Y_1 \\ \gamma^- Y_1 + \gamma^+ Y_2 - \rho^- Y_2 \\ -\beta \frac{Y_1 Y_3}{N} + \rho^- Y_2 \\ \alpha Y_1 - \gamma^+ Z_1 \end{pmatrix}, \quad \sigma(t, X(t)) = \begin{pmatrix} \sqrt{\beta \frac{Y_1 Y_3}{N}} & -\sqrt{\gamma^- Y_1} & 0 & -\sqrt{\alpha Y_1} & 0 \\ 0 & \sqrt{\gamma^- Y_1} & -\sqrt{\rho^- Y_2} & 0 & \sqrt{\gamma^+ Z_1} \\ -\sqrt{\beta \frac{Y_1 Y_3}{N}} & 0 & \sqrt{\rho^- Y_2} & 0 & 0 \\ 0 & 0 & 0 & \sqrt{\alpha Y_1} & -\sqrt{\gamma^+ Z_1} \end{pmatrix}.$$

This diffusion approximation can be written as

$$dY = \bar{f}(t, Y, Z)dt + \bar{\sigma}(t, Y, Z)dW^1 + \bar{g}(t, Y, Z)dW^2$$

$$dZ = [\bar{h}_0(t, Z) + \bar{h}_1(t, Z)Y]dt + \bar{\ell}(t, Y, Z)dW^2$$

where the first equation represents is the SDE for the hidden sate  $Y$ , the second equation is the SDE for the observable state. The coefficients  $\bar{f}$ ,  $\bar{\sigma}$ ,  $\bar{g}$ ,  $\bar{\ell}$  are non-linear in the hidden state  $Y$  and given as follow

$$\bar{f}(t, Y, Z) = \begin{pmatrix} \beta \frac{Y_1 Y_3}{N} - (\gamma^- + \alpha)Y_1 \\ \gamma^- Y_1 - \rho^- Y_2 + \gamma^+ Z_1 \\ -\beta \frac{Y_1 Y_3}{N} + \rho^- Y_2 \end{pmatrix}, \quad \bar{\sigma}(t, Y, Z) = \begin{pmatrix} \sqrt{\beta \frac{Y_1 Y_3}{N}} & -\sqrt{\gamma^- Y_1} & 0 \\ 0 & \sqrt{\gamma^- Y_1} & -\sqrt{\rho^- Y_2} \\ -\sqrt{\beta \frac{Y_1 Y_3}{N}} & 0 & \sqrt{\rho^- Y_2} \end{pmatrix},$$

$$\bar{g}(t, Y, Z) = \begin{pmatrix} -\sqrt{\alpha Y_1} & 0 \\ 0 & \sqrt{\gamma^+ Z_1} \\ 0 & 0 \end{pmatrix}, \quad \bar{h}_0(t, Z) = -\gamma^+ Z_1,$$

$$\bar{h}_1(t, Z) = (\alpha \ 0 \ 0), \quad \bar{\ell}(t, Y, Z) = (\sqrt{\alpha Y_1} - \sqrt{\gamma^+ Z_1})$$

## 4.2 Measles Model

Measles, also known as rubeola, is a highly contagious viral disease caused by the Measles morbillivirus. I When a person is infected, they move to the exposed compartment ( $E$ ), and the progression from exposure to recovery can be summarized in three stages. The first stage is the incubation period, which lasts 7 – 14 days. During this period there is no symptoms and the individual is not yet infectious [25]. The second stage is characterized by the initial symptoms follow by the rash. During this period the infected individual is infectious and can transmit the virus to a susceptible person. The last stage concern the recovery stage. Here most of the people fully recovered within 2 – 3 weeks of the rash appearing. Knowing that during the second stage, it is crucial to isolate the infected person to prevent spreading the virus to others and also since there is no specific treatment for the measles we will assume that detected infected individuals  $I^+$  stay in quarantine and consequently have no contact with other susceptible person. Vaccination, in particular the highly effective MMR (measles, mumps and rubella) vaccine, is the most effective way of preventing measles, as the herd immunity resulting from widespread vaccination is crucial to preventing epidemics. In addition, recovering from the disease naturally grants lifelong immunity.

Many previous studies have relied on a modified SIERV-type models[[16],[33],[44]] to describe how measles spreads within a population. These models typically assume all compartments (susceptible, infected, exposed, recovered, vaccinated) are fully observable, which isn't always realistic because we have some compartment like the exposed compartment ( $E$ ) whose individuals are not directly observable. In this section we propose a modified stochastic SEIRV-epidemic model that takes into account the challenges of unobserved compartments, offering a more accurate representation of real-world scenarios.

We want to take into account some important characterization of the measles disease. The

first is the number of exposed individuals who later on will developed symptoms and become infectious. The second group consists of individuals who either refuse to take the test despite showing measles symptoms or are unaware of the significance of those symptoms. These individuals pose a critical challenge in the fight to eradicate the disease because they are highly infectious. If the number of undetected and infected cases rises, it would undermine the government's efforts to eliminate the disease. We divide the infected group into two:  $I^-$  the non-detected individuals, most often symptomatic and contagious, and  $I^+$  the detected part of the infected individuals. The most common methods for confirming a measles infection include serology (blood tests) and PCR (Polymerase Chain Reaction). Serology tests involve the IgM antibody test, which detects measles-specific IgM antibodies, indicating a current or recent infection. The PCR methods, specifically RT-PCR (Reverse Transcription PCR), detect the genetic material of the measles virus in clinical samples such as throat swabs, nasopharyngeal swabs, urine, or blood, offering high sensitivity and the ability to confirm infection even before antibodies are detectable.

#### 4.2.1 Compartments and Transitions

More specifically, all possible connections with random transitions can be visualized in the Figure 4.2. In addition, the parameters for the dynamics are described in the Table 4.2 and the all the transitions are given in Table 4.2.

**$E$ : non-detected exposed.** These individuals are asymptomatic, not sick and remain non-detected. After some days they will develop symptoms and move to  $I^-$ . Furthermore, since most of the individuals in this compartment are unaware of their exposed status, with the availability of the vaccine they will receive it as they are considered susceptible and move to the vaccinated compartment  $V$ .

**$I^-$ : non-detected infected.** These individuals are symptomatic, not sick enough to go to hospital and remain non-detected. They may either get tested and then move on to  $I^+$ , stay isolated, fully recover and develop full immunity or stay there and recover naturally. Furthermore, due to sudden events such as conflicts and humanitarian crises, many individuals in this compartment may be unaware of their infection status despite the awareness of measles. As they develop symptoms, they will likely wait until they fully recover and then consider as recovered non detected  $R^-$ .

**$R^-$ : recovered non-detected.** These individuals recovered from the disease without being informed of their infection. Since immunity is not lost over time, they will become immunized and either stay in  $R^-$  or move to  $V$  with the availability of the vaccine.

**$S$ : susceptible.** They can be infected by unquarantined infectious individuals, i.e. individuals in  $I^-$ . When susceptible individuals are infected, they move to  $E$ . And when they received the vaccine they move to  $V$ .

**$I^+$ : detected infected.** People who test positive are considered infected and detected. Once they test positive, they are placed in quarantine until they fully recover and then move into the  $R^+$  compartment as confirmed recovered. In this model, it is assumed that infected and detected individuals  $I^+$  cannot transmit the virus to others because they are effectively isolated.

$R^+$  : **recovered detected.** Here we consider individuals in this compartment are fully immune. They have a long life immunity.

$V$  : **vaccinated.** People considered for vaccination are susceptible  $S$ , exposed  $E$ , and recovered non-detected  $R^-$ . Since most of these people have no symptoms, they will be vaccinated. After vaccination, they develop full immunity against the future measles virus. The dynamics of this model 4.2 can be described using CTMC-model, where the transition

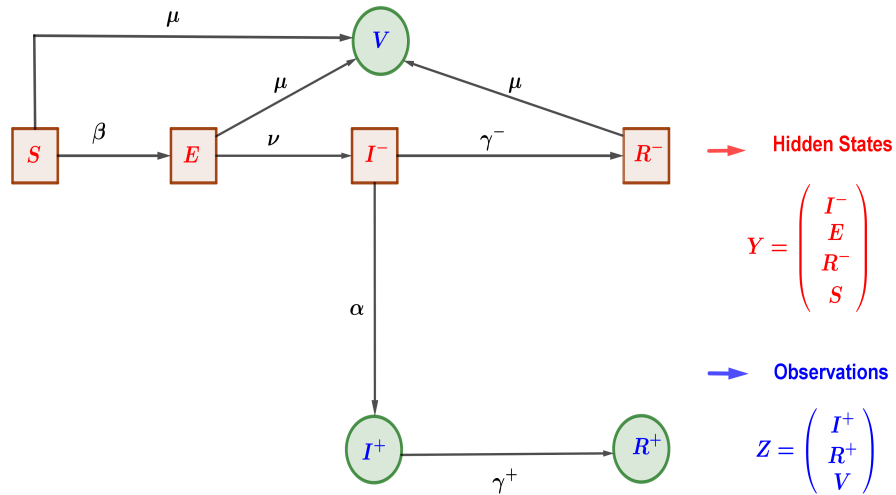


Fig. 4.2: Measles model with partial information; 4 fully hidden states :  $I^-, R^-, E, S$ ; 3 observable states :  $(I^+, R^+, V)$

vectors and intensities can be summarized as follows.

Consider a decomposition of the state process  $X$  into two components:  $Y$  and  $Z$  such that  $X = (Y, Z)$ . The component  $Y$  represents the hidden states, while  $Z$  model the observable part. corresponds to the observable states. In the context of the measles model, we define  $Y = (I^-, R^-, E, S)^\top$  which includes non directly observable variables and  $Z = (I^+, R^+, V)^\top$ , including directly observable quantities.

Table 4.2: Measles model : State process  $X$ ; Total number of states  $d = 7$ , Total transitions  $K = 9$ . Some the parameters as  $\beta, \mu$  and  $\alpha$  might be time-dependent.

k	Transition	Transition vectors $\xi_k$	intensity $\lambda_i(X)$
1	Exposed individuals become infectious	$(1, 0, -1, 0, 0, 0, 0)^\top$	$\nu E = \nu Y_3$
2	Recovering of infected detected	$(0, 0, 0, 0, 0, -1, 1)^\top$	$\gamma^+ I^+ = \gamma^+ Z_1$
3	Recovering of infected non-detected	$(-1, 1, 0, 0, 0, 0, 0)^\top$	$\gamma^- I^- = \gamma^- X_1$
4	Vaccination of non-detected infected	$(-1, 0, 0, 0, 0, 1, 0)^\top$	$\mu I^- = \mu Y_1$
5	Vaccination of non-detected recovered	$(0, -1, 0, 0, 1, 0, 0)^\top$	$\mu I^- = \mu Y_1$
6	Vaccination of susceptible	$(0, 0, 0, -1, 1, 0, 0)^\top$	$\mu S = \mu Y_4$
7	Infection	$(0, 0, 1, -1, 0, 0, 0)^\top$	$\frac{\beta S I^-}{N} = \frac{\beta Y_4 Y_1}{N}$
8	Test of infected non-detected	$(-1, 0, 0, 0, 0, 1, 0)^\top$	$\alpha I^- = \alpha Y_1$
9	Vaccination of exposed individuals	$(0, 0, -1, 0, 1, 0, 0)^\top$	$\mu E = \mu Y_3$

The changes in the sizes of each compartment are assumed to follow the dynamics described by the following SDEs. Recall figure 4.2, which illustrates the transitions of individuals from one state to another. In this case, the state process is given as  $X(t)$  and the corresponding diffusion approximation can be given in the form of (3.9), where the drift and diffusion coefficient are as follows: given the state process with respect to the hidden state  $Y$  and the observable state  $Z$ , we obtain

$$F(t, Y, Z) = \begin{pmatrix} \nu Y_3 - (\alpha + \gamma^-) Y_1 \\ \gamma^- Y_1 - \mu Y_2 \\ \beta \frac{Y_1 Y_4}{N} - (\mu + \nu) Y_3 \\ -\beta \frac{Y_1 Y_4}{N} - \nu Y_4 \\ (Y_2 + Y_3 + Y_4) \mu \\ \alpha Y_1 - \gamma^+ Z_2 \\ \gamma^+ Z_2 \end{pmatrix} \text{ and } \sigma(t, Y, Z) = \begin{pmatrix} \sqrt{\nu Y_3} & -\sqrt{\gamma^- Y_1} & 0 & -\sqrt{\alpha Y_1} & 0 & 0 & 0 & 0 \\ 0 & \sqrt{\gamma^- Y_1} & 0 & 0 & -\sqrt{\mu Y_2} & 0 & 0 & 0 \\ -\sqrt{\nu Y_3} & 0 & \sqrt{\beta \frac{Y_1 Y_4}{N}} & 0 & 0 & -\sqrt{\mu Y_3} & 0 & 0 \\ 0 & 0 & -\sqrt{\beta \frac{Y_1 Y_4}{N}} & 0 & 0 & 0 & -\sqrt{\mu Y_4} & 0 \\ 0 & 0 & 0 & 0 & \sqrt{\mu Y_2} & \sqrt{\mu Y_3} & \sqrt{\mu Y_4} & 0 \\ 0 & 0 & 0 & \sqrt{\alpha Y_1} & 0 & 0 & 0 & -\sqrt{\gamma^+ Z_2} \\ 0 & 0 & 0 & 0 & 0 & 0 & 0 & \sqrt{\gamma^+ Z_2} \end{pmatrix}$$

The obtained diffusion approximation, can be written as

$$dY = \bar{f}(t, Y, Z) dt + \bar{\sigma}(t, Y, Z) dW^1 + \bar{g}(t, Y, Z) dW^2$$

$$dZ = [\bar{h}_0(t, Z) + \bar{h}_1(t, Z) Y] dt + \bar{\ell}(t, Y, Z) dW^2$$

where the first equation represents the SDE for the hidden state  $Y$ , the second equation is the SDE for the observable state. The coefficients  $\bar{f}$ ,  $\bar{\sigma}$ ,  $\bar{g}$ ,  $\bar{\ell}$  are non-linear in the hidden state  $Y$  and given as follow

$$\bar{f}(t, Y, Z) = \begin{pmatrix} \nu Y_3 - (\alpha + \gamma^-) Y_1 \\ \gamma^- Y_1 - \mu Y_2 \\ \beta \frac{Y_1 Y_4}{N} - (\mu + \nu) Y_3 \\ -\beta \frac{Y_1 Y_4}{N} - \nu Y_4 \end{pmatrix}, \bar{\sigma}(t, Y, Z) = \begin{pmatrix} \sqrt{\nu Y_3} & -\sqrt{\gamma^- Y_1} & 0 \\ 0 & \sqrt{\gamma^- Y_1} & 0 \\ \sqrt{-\nu Y_3} & 0 & \sqrt{\beta \frac{Y_4 Y_1}{N}} \\ 0 & 0 & -\sqrt{\beta \frac{Y_4 Y_1}{N}} \end{pmatrix},$$

$$\bar{g}(t, Y, Z) = \begin{pmatrix} -\sqrt{\alpha Y_1} & 0 & 0 & 0 & 0 \\ 0 & -\sqrt{\mu Y_2} & 0 & 0 & 0 \\ 0 & 0 & -\sqrt{\mu Y_3} & 0 & 0 \\ 0 & 0 & 0 & -\sqrt{\mu Y_4} & 0 \end{pmatrix}, \bar{h}_0(t, Z) = \begin{pmatrix} 0 \\ -\gamma^+ Z_2 \\ \gamma^+ Z_2 \end{pmatrix},$$

$$\bar{h}_1(t, Z) = \begin{pmatrix} 0 & \mu & \mu & \mu \\ \alpha & 0 & 0 & 0 \\ 0 & 0 & 0 & 0 \end{pmatrix}, \bar{\ell}(t, Y, Z) = \begin{pmatrix} 0 & \sqrt{\mu Y_2} & \sqrt{\mu Y_3} & \sqrt{\mu Y_4} & 0 \\ \sqrt{\alpha Y_1} & 0 & 0 & 0 & -\sqrt{\gamma^+ Z_2} \\ 0 & 0 & 0 & 0 & \sqrt{\gamma^+ Z_2} \end{pmatrix}.$$

### 4.3 Covid-19 Model

In this section, we are going to propose a mathematical model of the dynamics of the Covid-19 pandemic. We wish to take into account three important characteristics during the Covid-19 pandemic. The first is the high proportion of asymptomatic patients, and the low rate of use of tests in many countries, and the second is the category of individuals who develop symptoms of the disease and are confirmed to be positive for the disease unofficially (i.e. through rapid tests obtained from local stores), but for one reason or another refuse to go to a testing center to confirm whether or not they are infected. The latter is thus a crucial problem in the fight to eradicate the disease, because if their numbers were to increase, we would be facing an outbreak of infectious individuals, which would compromise the government's efforts to eradicate the disease. We will divide the infected group ( $I$ ) into two:  $I^-$  the non-detected individuals, most often asymptomatic but contagious, and  $I^+$  the detected part of the infected individuals. During the Covid-19 pandemic, three main types of tests have been widely used for diagnosing the virus.

The first two on the list are tests that can be used to confirm the presence or absence of the Covid-19 virus. These are PCR tests (Polymerase Chain Reaction): PCR tests are considered the gold standard for Covid-19 diagnosis. They detect the virus' genetic material and are highly accurate. However, they can take from a few hours to a few days to produce results, depending on laboratory capacity and test volume. In addition, we have antigenic tests. These tests detect specific proteins on the surface of the virus. They are faster and less expensive than PCR tests, but may be slightly less sensitive. Antigenic tests are often used for rapid screening in settings where immediate results are needed, such as workplaces, schools and community testing sites. Results can be available in less than 15 to 30 minutes. The third is an antibody test. They detect the antibodies produced by the body in response to an infection with Covid-19. These tests can indicate whether a person has already been infected with the virus, i.e. they are used to detect whether a person has previously recovered from a Covid-19 infection. Unfortunately, antibody tests could not provide information on immunity levels or protection against reinfection [24], limiting their usefulness for public health decision-making. Consequently, the focus shifted to tests that could diagnose active infections, such as PCR and antigenic tests, which were more important for controlling the spread of the virus.

When a given person is tested as a positive individual, he moves from the  $I^-$  to  $I^+$ . Additionally, we also split the recovered compartment into two different compartments:  $R^-$  the non detected recovered and  $R^+$  the detected recovered.  $R^-$  collects recovered individuals from  $I^-$  while  $R^+$  those recovered from  $I^+$ . An important feature of a pandemic such as Covid-19 is the problem highlighted by the concept of "flattening the curve" (discussed in [47] and [22]), which means that one of the objectives of choosing a public health intervention should be to avoid an increase in demand in the healthcare system, and in particular in intensive care units. From a modeling point of view, we incorporate several compartments to represent different population groups based on their interactions with the healthcare system and vaccination status. First, we introduce the compartments  $H$  (hospitalized individ-

uals) and  $C$  (individuals requiring intensive care units, ICUs). These compartments allow us to distinguish between those utilizing healthcare services based on the severity of their illness. The  $C$  compartment captures critically ill patients who require ICU support, reflecting the strain on critical care resources. In addition, due to the availability of vaccines, we include a vaccinated compartment  $V$ . This compartment aggregates all individuals who have received at least one dose of the vaccine, regardless of the number of doses or the vaccine type administered. This simplifies the model by not distinguishing between partially and fully vaccinated individuals, focusing instead on the collective impact of vaccination on disease dynamics. As none of the available Covid-19 vaccines (i.e, mRNA Vaccines: mRNA vaccines, such as the Pfizer-BioNTech, Moderna vaccines,...etc.) offer lifelong immunity, it's possible for vaccinated individuals to lose their immunity over time and become susceptible. We also assume that in this model, deaths due to Covid-19 occur exclusively among individuals in the  $C$  compartment, simplifying the representation of fatality risks. Finally, the  $D$  (death) compartment accounts for those who succumb to the disease. This structure captures key aspects of healthcare system interaction, vaccination impact, and disease outcomes, offering a framework to analyze epidemic dynamics and potential policy interventions.

### 4.3.1 Compartments and Transitions

More specifically, all possible states connected with random transition can be visualized on figure 4.3.

**$I^-$  : non-detected infected.** These individuals may be asymptomatic, not sick enough to go to hospital and remain undetected. They may either get tested (with PCR tests, then move on to  $I^+$ ), become sicker and go to hospital  $H$ , or simply recover and develop partial immunity, but remain non-detected  $R^-$  after loosing immunity they will become susceptible. Additionally, many individuals in this compartment are either unaware of their infection status or choose to stay calm" and "hide" knowing they are infected. With the introduction of the vaccine, they will be vaccinated as they are classified as susceptible.

**$R^-$  : recovered non-detected..** These individuals recovered from the disease which has not been detected. Since immunity is lost over time, some will become susceptible while others will receive the vaccine.

**$S$ : susceptible.** They can be infected by unquarantined infectious individuals, i.e. individuals in  $I^-$ . When susceptible individuals are infected, they move to  $I^-$ . And when they received the vaccine they move to  $V$ . In addition, it is possible to have been infected and then recovered from the disease and lost immunity.

**$I^+$  : infected detected.** People who tested positive but are not hospitalized are considered infected and detected. They have two options: either they get worse and have to be hospitalized  $H$ , or they recover and move into the  $R^+$  compartment as confirmed cases. In this model, it is assumed that individuals in  $I^+$  cannot transmit the virus to others, as they are effectively isolated.

**$R^+$  : recovered detected.** Individuals in this compartment recovered from the disease which has been detected may lose their immunity and become susceptible again.



**H: Hospitalized** . All people admitted to hospital are tested. They have two options: either their condition deteriorates and they require intensive care  $C$ , or they recover and move into the  $R^+$  compartment. It is important to note that hospitalization  $H$  represents an intermediate state between infection and becoming seriously ill or succumbing to the disease. The direct transition from infected individuals but not in hospital ( $I^-, I^+$ ) to the deceased  $D$  state is not possible.

**C: Intensive care hospitalization.** This for people at an advanced (and detected) stage of the disease, requiring ventilators and specialized medical care. Patients in this unit are transferred from the ( $H$ ) unit and face two possible outcomes: they may recover and move to the ( $R^+$ ) compartment, or they may succumb to the disease and move to the deceased category ( $D$ ).

**D: death, from disease.** We assume that only hospitalized patients, especially those in intensive care, are likely to die of the disease. They form the  $D$  compartment.

**V : vaccinated.** People who receive the vaccine are susceptible ( $S$ ), infected but not detected (asymptomatic) ( $I^-$ ) and recovered but not detected ( $R^-$ ). Since most of these people have very few or no symptoms, they will go for and admitted vaccination. After vaccination, they will gradually lose their immunity, returning to a susceptible state.

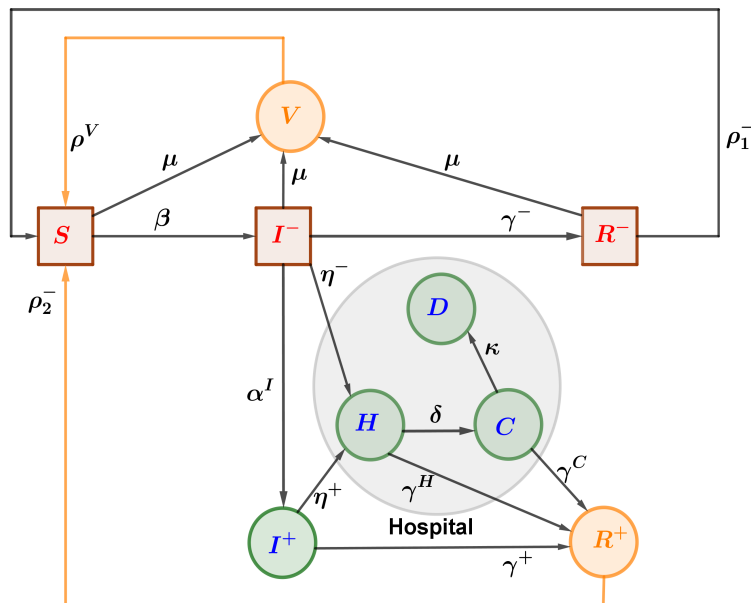


Fig. 4.3: Covid-19 model with partial information; 3 fully hidden states :  $I^-, R^-, S$ ; 2 partially hidden states :  $R^+, V$ ; 4 observation states :  $(I^+, H, C, D)$ .

In Figure 4.3, "fully hidden states" refer to states where both the inflow and outflow are observable, while "partially hidden states" refer to those where either the inflow or the outflow is observable, but not both.

#### 4.4 Diffusion Approximation of Covid-19 Model

The dynamics of the Covid-19 model 4.3 can be described using CTMC, where the transition vectors and intensities are given in Table 4.3.

Based on the information in Table 4.3, we can express the dynamics of the state process

Table 4.3: Covid-19 model without considering partially observed compartments ( $V$  and  $R^+$ ): State process  $X = \begin{pmatrix} Y \\ Z \end{pmatrix}$ ,  $Y = (I^-, R^-, R^+, V, S)^\top$ ,  $Z = (I^+, H, C, D)^\top$ ; Total number of states  $d = 9$ , Total transitions  $K = 16$ .

k	Transition	Transition vectors $\xi_k$	Intensity $\lambda_i(t, X)$
1	Infection of susceptible	$(1, 0, 0, 0, -1, 0, 0, 0, 0)^\top$	$\beta S \frac{I^-}{N} = \beta Y_5 \frac{Y_1}{N}$
2	Test of infected non-detected	$(-1, 0, 0, 0, 0, 0, 1, 0, 0, 0)^\top$	$\alpha I^- = \alpha Y_1$
3	Recovering of infected detected	$(0, 0, 1, 0, 0, -1, 0, 0, 0)^\top$	$\gamma^+ I^+ = \gamma^+ Z_1$
4	Recovering of infected non-detected	$(-1, 1, 0, 0, 0, 0, 0, 0, 0)^\top$	$\gamma^- I^- = \gamma^- Y_1$
5	Losing immunity of detected recovered	$(0, 0, -1, 1, 0, 0, 0, 0, 0)^\top$	$\rho_2^- R^+ = \rho_2^- Y_3$
6	Losing immunity of non-detected recovered	$(0, -1, 0, 1, 0, 0, 0, 0, 0)^\top$	$\rho_1^- R^- = \rho_1^- Y_2$
7	Losing immunity of vaccinated	$(0, 0, 0, -1, 1, 0, 0, 0, 0)^\top$	$\rho^V V = \rho^V Y_4$
8	Vaccination of non-detected infected	$(-1, 0, 0, 0, 1, 0, 0, 0, 0)^\top$	$\mu I^- = \mu Y_1$
9	Vaccination of non-detected recovered	$(0, -1, 0, 0, 1, 0, 0, 0, 0)^\top$	$\mu R^- = \mu Y_2$
10	Vaccination of susceptible	$(0, 0, 0, 1, -1, 0, 0, 0, 0)^\top$	$\mu S = \mu Y_5$
11	Hospitalization of non-detected infected	$(-1, 0, 0, 0, 0, 0, 1, 0, 0)^\top$	$\eta^- I^- = \eta^- Y_1$
12	Hospitalization of detected infected	$(0, 0, 0, 0, 0, -1, 1, 0, 0)^\top$	$\eta^+ I^+ = \eta^+ Z_1$
13	Recovering from Hospitalization	$(0, 0, 1, 0, 0, 0, -1, 0, 0)^\top$	$\gamma^H H = \gamma^H Z_2$
14	Recovering from ICU	$(0, 0, 1, 0, 0, 0, 0, -1, 0)^\top$	$\gamma^C C = \gamma^C Z_3$
15	Transfer to ICU	$(0, 0, 1, 0, 0, 0, -1, 0, 0)^\top$	$\delta H = \delta Z_2$
16	Death	$(0, 0, 1, 0, 0, 0, 0, -1, 1)^\top$	$\kappa C = \kappa Z_3$

as a CTMC as described in Section 2.1, Equation (2.1) and based in the result in Section 3.4, we can write down our state dynamic by Equation (3.6). The changes in the sizes of each compartment are assumed to follow the dynamics described by a system of stochastic differential equations. In this case the state process is given as  $X$ , and the corresponding diffusion approximation is given in appendix C.1. This diffusion approximation can be written as

$$dY = \bar{f}(t, Y, Z)dt + \bar{\sigma}(t, Y, Z)dW^1 + \bar{g}(t, Y, Z)dW^2$$

$$dZ = [\bar{h}_0(t, Z) + \bar{h}_1(t, Z)Y]dt + \bar{\ell}(t, Y, Z)dW^2$$

where the first equation represents the SDE for the hidden state  $Y$ , the second equation is the SDE for the observable state. The coefficients  $\bar{f}$ ,  $\bar{\sigma}$ ,  $\bar{g}$ ,  $\bar{\ell}$  are non-linear in the hidden state  $Y$  and given as follows

$$\bar{f}(t, Y, Z) = \begin{pmatrix} \beta \frac{Y_1 Y_5}{N} - (\alpha + \gamma^+ + \eta^- - \mu) Y_1 \\ \gamma^- Y_1 - \mu Y_2 - \rho_1^- Y_2 \\ \gamma^+ Z_1 + \gamma^H Z_2 + \gamma^C Z_3 - \rho_2^- Y_3 \\ (Y_1 + Y_2 + Y_5) \mu - \rho^V Y_4 \\ -\beta \frac{Y_1 Y_5}{N} - \mu Y_5 + \rho_1^- Y_2 + \rho_2^- Y_3 + \rho^V Y_4 \end{pmatrix},$$

$$\bar{\sigma}(t, Y, Z) = \begin{pmatrix} \sqrt{\beta \frac{Y_1 Y_5}{N}} & -\sqrt{\gamma^- Y_1} & \sqrt{\mu Y_1} & 0 & 0 & 0 & 0 & 0 \\ 0 & \sqrt{\gamma^- Y_1} & 0 & -\sqrt{\mu Y_2} & -\sqrt{\rho_1^- Y_2} & 0 & 0 & 0 \\ 0 & 0 & 0 & 0 & 0 & -\sqrt{\rho_2^- Y_3} & 0 & 0 \\ 0 & 0 & \sqrt{\mu Y_1} & \sqrt{\mu Y_2} & 0 & 0 & \sqrt{\mu Y_5} & -\sqrt{\rho^V Y_4} \\ -\sqrt{\beta \frac{Y_1 Y_5}{N}} & 0 & 0 & 0 & \sqrt{\rho_1^- Y_2} & \sqrt{\rho_2^- Y_3} & -\sqrt{\mu Y_5} & \sqrt{\rho^V Y_4} \end{pmatrix}$$

$$\bar{g}(t, Y, Z) = \begin{pmatrix} -\sqrt{\alpha Y_1} - \sqrt{\eta^- Y_1} & 0 & 0 & 0 & 0 & 0 & 0 & 0 \\ 0 & 0 & 0 & 0 & 0 & 0 & 0 & 0 \\ 0 & 0 & \sqrt{\gamma^+ Z_1} & \sqrt{\gamma^H Z_2} & \sqrt{\gamma^C Z_3} & 0 & 0 & 0 \\ 0 & 0 & 0 & 0 & 0 & 0 & 0 & 0 \\ 0 & 0 & 0 & 0 & 0 & 0 & 0 & 0 \end{pmatrix},$$

$$\bar{h}_0(t, Z) = \begin{pmatrix} -\gamma^+ Z_1 - \eta^+ Z_1 \\ \eta^+ Z_1 - \delta Z_2 - \gamma^H Z_2 \\ \delta Z_2 - \gamma^C Z_3 - \kappa Z_3 \\ \kappa Z_3 \end{pmatrix}, \bar{h}_1(t, Z) = \begin{pmatrix} \alpha & 0 & 0 & 0 & 0 \\ \eta^- & 0 & 0 & 0 & 0 \\ 0 & 0 & 0 & 0 & 0 \\ 0 & 0 & 0 & 0 & 0 \end{pmatrix},$$

$$\bar{\ell}(t, Y, Z) = \begin{pmatrix} \sqrt{\alpha Y_1} & 0 & -\sqrt{\gamma^+ Z_1} & 0 & 0 & -\sqrt{\eta^+ Z_1} & 0 & 0 \\ 0 & \sqrt{\eta^- Y_1} & 0 & -\sqrt{\gamma^H Z_2} & 0 & 0 & 0 & -\sqrt{\delta Z_2} \\ 0 & 0 & 0 & 0 & -\sqrt{\gamma^C Z_3} & 0 & -\sqrt{\kappa Z_3} & \sqrt{\delta Z_2} \\ 0 & 0 & 0 & 0 & 0 & 0 & \sqrt{\kappa Z_3} & 0 \end{pmatrix}$$

#### 4.5 Cascade State Modeling

In the model described in Figure 4.3 we have a total of  $K = 16$  random transitions and  $d = 9$  compartments. In particular, there are two compartments highlighted in orange in this figure: the recovered and the vaccinated compartments. These compartments have a unique feature in that they are partially observed compartments. Specifically, both have observable inflows and unobservable outflows. For example, in the case of the recovered compartment, there are three different inflows: from individuals recovering from  $I^+$ ,  $H$  and  $C$  respectively. These inflows are observable because we can track individuals recovering from hospital and quarantine. However, the outflow, which represents individuals who lose immunity, remains unknown and unobservable because we have no information on the timing of immunity loss. Thus, while we know the inflow, we lack information on when individuals will leave the compartment due to loss of immunity. Similarly, for the

vaccinated compartment, we can document individuals receiving the vaccine, but the timing of immunity loss remains uncertain. To make better use of the available information, we propose to divide each compartment into two distinct groups: an observable part and an unobservable part. The unobservable part, called the hidden compartment with waning immunity, represents those individuals within the recovered and vaccinated compartments whose status cannot be directly observed. On the other hand, for the observable part, we want to divide it into  $L^G$  sequential or cascade compartments. We assume perfect immunity for a known period of time, which is divided into  $L^G$  sub-periods. These cascading compartments are used to model the progressive loss of immunity over time for both recovered and vaccinated individuals.

In certain epidemic models with hidden states, some compartments may have one or more observable incoming transitions, while their outgoing transitions may be partially or completely unobservable. As a result, these compartments are treated as hidden. To extract useful information from the observed incoming transitions, the compartment can be divided into a sequence of generic sub-compartments, denoted as  $G_i$ , for  $i = 1, \dots, L^G$ . Each sub-compartment  $G_i$  groups individuals based on their time since entering the compartment, effectively tracking their  $G_i$  age. The number of sub-compartments  $L^G$  is typically chosen to match the period during which no outgoing transitions occur, such as the duration of full immunity following recovery or vaccination.

#### 4.5.1 Continuous-time Dynamics

Consider the diagram in Figure 4.4 where we assume a random observable inflow into the first generic compartment,  $G_1$ , and a non-observable outflow from the last compartment, denoted by  $G^-$ . Between these two compartments, we introduce  $L^G - 1$  additional compartments, representing different  $G$ -ages within the overall compartment  $G$ . Additionally, except for the random inflow and outflow, all transitions between compartments are deterministic. Let  $\tau_1, \dots, \tau_{L^G}$  represent the accounting dates, times at which individuals in each  $G_i$  compartment transition to the next. If the time spent in each compartment  $G_i$  is  $\Delta\tau = \tau_{i+1} - \tau_i$ , the dynamics from  $G_1$  to  $G^-$  can be described as in Figure 4.4.

Now, we assume that the state process  $X$  can be decomposed into  $(X^e, G)$ , where  $X^e$  con-

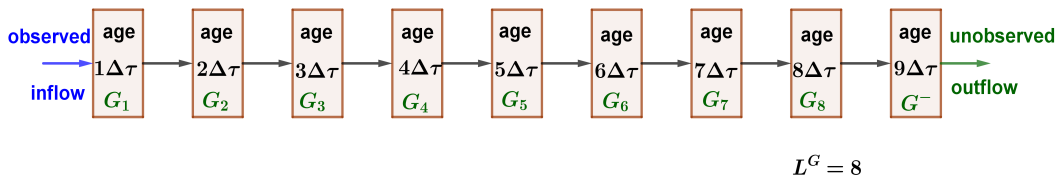


Fig. 4.4: Cascade state illustration with 8 compartment ( $G_l, l = 1 \dots, L^G = 8$ );  
observed inflow : random inflow in the compartment 1 ( $G_1$ ) with  $G$ -age,  $1\Delta\tau$ ,  
non-observed outflow : random outflow from the compartment  $G^-$  with  $G$ -age,  $\geq 9\Delta\tau$   
Between  $G_1$  and  $G^-$ , only deterministic transition.

tains the  $d^e < d$  traditional states with random inflow or outflow, and  $G$  contains the  $L^G$  new states with deterministic transitions.

Let us consider the microscopic CTMC model given in Equation (2.1) but restrict this point of view to the time intervals  $[0, T]$ . To account for transitions between cascade states,

we introduce additional counting processes, denoted as  $M_k(t)$ ,  $k = K + 1, \dots, K + L^G$ , which track the total number of transitions in the time interval  $[0, T]$  between compartments  $G_1, \dots, G_{L^G}$ . These processes share some similarities with traditional Poisson counting processes, but also key differences. Like Poisson processes,  $M_k(t)$ ,  $k = K + 1, \dots, K + L^G$  start at zero at  $t = 0$  and are piecewise constant. Unlike traditional Poisson processes, the jump times of  $M_k(t)$ ,  $k = K + 1, \dots, K + L^G$ , are fixed and occur only at the predetermined, non-random counting dates  $\tau_l$ . Instead of a constant jump size of 1, the jumps represent the number of individuals transitioning between cascade compartments and are thus state-dependent. The introduction of  $M_k(t)$   $k = K + 1, \dots, K + L^G$ , naturally extends the existing model dynamics. These processes can be incorporated into the traditional Poisson process framework as follows:

$$X(t) = X(0) + \sum_{k=1}^{K+L^G} \xi_k M_k(t), \quad t \in [0, T]$$

where the transition vectors  $\xi_k$ , and the counting process  $M_k$ ,  $k = 1, \dots, K$ , referring to the random transitions (but not to the deterministic transitions between the new additional sub-compartment) and the transition vectors  $\xi_k$ , and the counting process  $M_k$ ,  $k = K + 1, \dots, K + L^G$ , referring to the deterministic transitions between the new additional sub-compartment. For  $k = K + 1, \dots, K + L^G$ ,  $\xi_k$  are transition vectors with entries  $+1$  (for deterministic inflow) and  $-1$  (for outflow) for each cascade compartment. These cumulative jump processes provide a more detailed view of transitions within cascade states. The additional structure allows the model to capture the aggregated movement between compartments over time and also account for state-dependent transition magnitudes while maintaining deterministic jump times.

#### 4.5.2 Reduction of Additional Compartments and Diffusion Approximation

Without loss of generality, if we assume  $\Delta \tau = 1$  day, we can define compartments  $G_k$  for individuals who have spent  $k$  days in  $G^-$  between two accounting dates. However, this would create an excessive number of sub-compartments. To simplify, we aggregate  $P_k \in \mathbb{N}$  consecutive daily sub-compartments into a single one. Thus,  $G_1$  includes individuals with a  $G$ -age between 1 and  $P_1$  days,  $G_2$  covers those from  $P_1 + 1$  to  $P_2$  days, and so forth, up to  $G_{L^G}$ , which includes individuals aged  $P_{L^G-1} + 1$  to  $P_{L^G}$  days. This approximation leads to the relation:  $L^G = \sum_{k=1}^{\bar{K}} P_k$ , with  $P_k \in \mathbb{N}$  and  $\bar{K}$  the total number of aggregation. Figure 4.5 illustrates that, by introducing a total of nine additional compartments, different groupings can be applied based on the chosen modeling approach. Notably, the sizes of groups  $P_k$  may vary, as depicted in Figure 4.5. In the following  $G_k$ ,  $k = 1, \dots, \bar{K}$  will represent the collection of  $P_k$  individuals. Therefore, the exact dynamics can be expressed in the form

$$G_k(\tau_l) = G_k(\tau_{l-}) - M_k(\tau_l) + M_{k-1}(\tau_l), \quad k = 1, \dots, \bar{K}$$

where:  $M_k(\tau_l)$  represents the number of individuals leaving compartment  $G_k$  at time  $\tau_l$ , corresponding to those who have reached the age threshold  $\Delta \tau \sum_{i=1}^k P_i$ .  $M_{k-1}(\tau_l)$  accounts

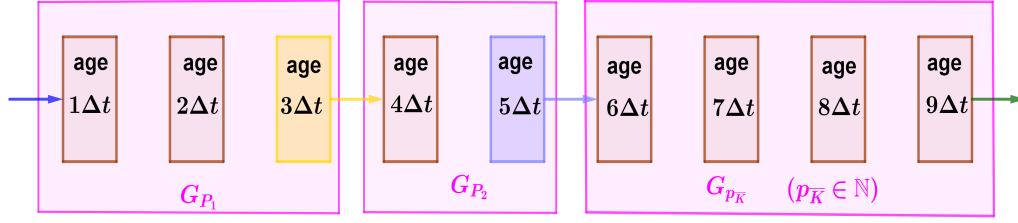


Fig. 4.5: Grouping of additional compartments:  $G_{P_k}$  groups together individuals with  $P_k$  neighbouring "G ages". Individual ages within a given group  $G_{P_k}$  are no longer distinguished.

for the number of individuals entering compartment  $G_k$  from  $G_{k-1}$ , having reached the age  $\Delta \tau \sum_{i=1}^{k-1} P_i$ .

This formulation naturally extends the model dynamics by explicitly incorporating the cascade structure of transitions through age-based compartments. One main idea when modeling the dynamics of individuals leaving a compartment, is to assume that for a small enough  $\Delta \tau$ , we can approximate the exact dynamic in a more formal form. Now, let us consider  $G_k(\tau_l)$ , the total number of individuals in the generic compartment  $G_k$  at the accounting date  $\tau_l$ . If we interpret the "outflow of  $x$  individuals from  $G_k$ " as a value for a time period, we aim to find a suitable approximation for the average number of individuals leaving the compartment  $G_k$ . The outflow in time step  $\Delta \tau$  represents the total number of individuals who leave the compartment  $G_k$ . Now if we consider  $\frac{G_k(\tau_l)}{P_k} \times \Delta \tau$ , it represents the outflows of individuals (on average) from  $G_k$  during  $\Delta \tau$ . It is justified especially under the assumption of non-distinguishable individuals in the compartment  $G_k$ .

Now we can approximate the exact dynamics when  $\Delta \tau = 1$  day in the following form

$$G_k(\tau_l) \approx G_k(\tau_{l-}) - M_k(\tau_l) + M_{k-1}(\tau_l),$$

By using this approximation, the recursive dynamics will adopt the subsequent structure:

$$X(t) = X(0) + \sum_{k=1}^{K+\bar{K}} \xi_k M_k(t), \quad t \in [0, T].$$

Taking the population limit  $N \rightarrow \infty$ , we derive from the law of large numbers:

$$\frac{d}{dt} \bar{X}(t) = \bar{F}_{\text{base}}(t, \bar{X}(t)) + \sum_{k=K+1}^{\bar{K}} \xi_k M_k(t), \quad t \in [0, T],$$

where:  $\bar{F}_{\text{base}}$  represents the baseline deterministic dynamics, derived from  $\bar{F}$ , excluding cascade states (see, (3.1)). The additional term  $\sum_{k=K+1}^{\bar{K}} \xi_k M_k(t)$  captures the discrete cascade transitions. By applying the CLT for Poisson processes, we obtain the following stochastic diffusion approximation:

$$dX^D(t) = F_{\text{base}}(t, X^D(t))dt + \sigma_{\text{base}}(t, X^D(t))dW(t) + \sum_{k=K+1}^{\bar{K}} \xi_k M_k(t), \quad t \in [0, T], \quad (4.1)$$

where:  $F_{\text{base}}$  and  $\sigma_{\text{base}}$  describe the drift and diffusion terms of the underlying dynamics without cascade states, constructed from  $F$  and  $\sigma$ , respectively (see, (3.9)). The summation term accounts for the additional stochastic contributions due to cascade transitions. This formulation clearly distinguishes between the baseline system dynamics and the effects introduced by cascade compartments while maintaining consistent notation.

### 4.5.3 Discrete-time Dynamics

We assume that the duration between two accounting dates matches  $\Delta t$ , representing a time step. Then, we can derive the a recursive dynamics for the number of individuals at a specific time  $n$  in each compartment  $G_i$ , where  $i = 1, \dots, L^G$ . Applying the Euler-Maruyama time discretization to the diffusion approximation given by the SDE,  $dX^D(t) = F_{\text{base}}(t, X^D(t))dt + \sigma_{\text{base}}(t, X^D(t))dW(t)$ , with the discrete time points equal to  $\tau_0, \tau_1, \dots$  (accounting dates) or containing these dates as a subset leads to the corresponding discrete-time dynamics. Now for discrete time points  $t_n = \tau_n$ , we obtained that

$$\begin{aligned} G_1(t_{n+1}) &= G^I \\ G_{k+1}(t_{n+1}) &= G_k(t_n), \quad k = 1, \dots, L^G - 2 \\ G_L(t_{n+1}) &= G_L^G(t_n) + G_{L^G-1}(t_n) - G^O, \end{aligned}$$

where,  $G^I$  is the and the inflow in  $[t_n, t_{n+1})$  and  $G^O$  the outflow in  $[t_n, t_{n+1})$ . We proceed with the grouping of  $P_k > 1$  days, and based on the approximation from section 4.5.2, we set  $\psi_k = \frac{1}{P_k}$ ,  $k = 1, \dots, \bar{K}$ , then the recursive dynamics will adopt the subsequent structure :

$$\begin{aligned} G_1(t_{n+1}) &= (1 - \psi_1)G_1(t_n) + G^I, \\ G_2(t_{n+1}) &= (1 - \psi_2)G_2(t_n) + \psi_1 G_1(t_n), \\ &\vdots \\ G_{\bar{K}}(t_{n+1}) &= (1 - \psi_{\bar{K}})G_{\bar{K}}(t_n) + \psi_{\bar{K}} G_{\bar{K}-1}(t_n), \\ G^-(t_{n+1}) &= G^-(t_n) + \psi_{\bar{K}} G_{\bar{K}}(t_n) - G^O. \end{aligned}$$

The time-discretized version of the model dynamics in equation (4.1) follows the general form:

$$X_{n+1} = X_n + F_{\text{base}}(n, X_n)\Delta t + \sigma_{\text{base}}(n, X_n)\sqrt{\Delta t}\mathcal{E}_{n+1} + \bar{A}_X X_n \quad (4.2)$$

where

$$\bar{A}_X = \begin{bmatrix} 0_{de} & 0 \\ 0 & \bar{A}_V \end{bmatrix}, \quad \bar{A}_V = \begin{bmatrix} -\psi_1 & 0 & 0 & \dots & 0 & 0 \\ \psi_1 & -\psi_2 & 0 & \dots & 0 & 0 \\ 0 & \psi_2 & -\psi_3 & 0 & \dots & 0 \\ 0 & \dots & \ddots & \ddots & \vdots & \vdots \\ 0 & \dots & \dots & \dots & \psi_{\bar{K}-1} & -\psi_{\bar{K}} \\ 0 & \dots & \dots & \dots & \psi_{\bar{K}} & 0 \end{bmatrix}$$

and  $X_n$  is of the form  $X_n = (X_n^e, G_n)$ .

#### 4.6 Covid-19 Modeling with Cascade States

Here, we consider an extension of the model presented in 4.3, introducing additional cascade compartments to capture information from various inflows into compartments  $R^+$  and  $V$  named as partially hidden states.

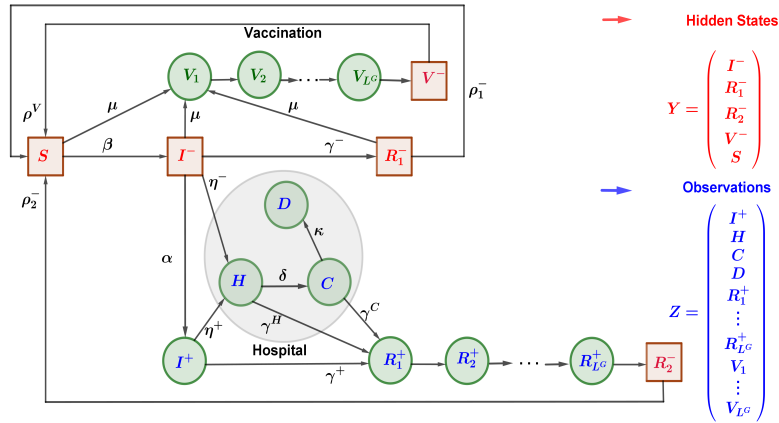


Fig. 4.6: Covid-19 model with partial information: 5 hidden states ( $I^-, R_1^-, R_2^-, V^-, S$ ) and  $2L + 4$  observable states, including  $2L$  cascade states ( $R_i^+, V_i, i = 1, 2, L$ ) and 4 other observable states including hospital ( $I^+, H, C, D$ ).

In order to make the information from the observable random transitions available for the estimation (filtering) of the hidden states, the idea is to split compartments with observable random inflow into a sequence of additional compartments. For example according to the Figure 4.6, we split the sub-population of vaccinated and recovered and detected individuals ( $V$  and  $R^+$ ) into  $V_1, \dots, V_{L^c}, V^-$  and  $R_1^+, \dots, R_{L^c}^+, R_2^-$  receptively.

Based on the information provided, the number of additional compartments required for modeling a person recovering from the disease depends on the duration considered for recovery, relative to the time step. For instance, if recovery without fading immunity



is assumed to occur over  $L^R$  time units (e.g.,  $L^R = 30$  days) and the time step is set to 1 day, this would necessitate the addition of up to 30 extra compartments. While this approach offers an advantage in modeling immunity loss (as described in Figure 4.6), it also introduces significant complexity to the model. To mitigate this complexity, we initially grouped certain compartments together, assuming that all individuals within each group were indistinguishable. We assume that immunity begins to decline 90 days after vaccination or recovery. To model this, we divide this period into three compartments, each consisting of 30 days. As a result, we obtain three sequential compartments, representing either the recovery process or the vaccination process with perfect immunity. During these 90 days, whether after vaccination or simple recovery, it is impossible for a person to become susceptible. According to our proposed model, we define  $\psi_1 = \psi_2 = \psi_3 = \frac{1}{30}$ . We then obtain the following proposed Covid-19 model 4.7.

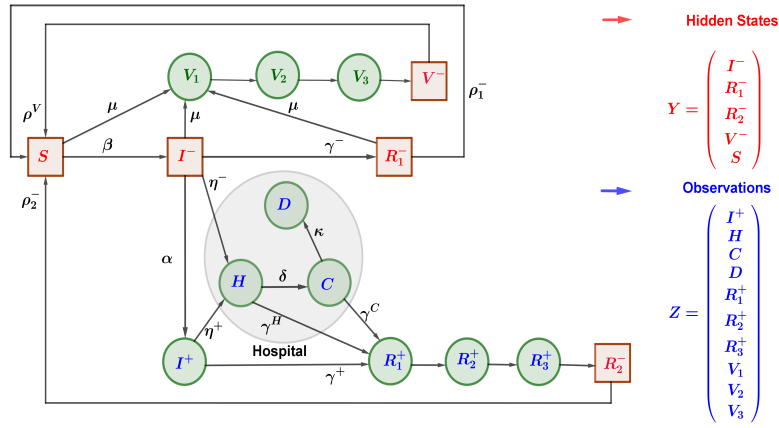


Fig. 4.7: Covid-19 model with partial information; 5 hidden states :  $I^-, R_1^-, R_2^-, S, V^-$ ; 10 observable states : 6 cascade states ( $R_i^+, V_i, i = 1, 2, 3$ ) and 4 observable states including hospital ( $I^+, H, C, D$ );

The evolution of subpopulation sizes within each compartment is governed by a system of SDEs, complemented by deterministic equations that describe the cascade dynamics.

In this framework, the full state process is structured as  $X = \begin{pmatrix} Y^e \\ Y^G \\ Z^e \\ Z^G \end{pmatrix}$ , where the hidden

and observable states are decomposed as follows: the core epidemic compartments are

given by  $X^e = \begin{pmatrix} Y^e \\ Z^e \end{pmatrix}$  with  $Y^e = \begin{pmatrix} I^- \\ R_1^- \\ S \end{pmatrix}$  and  $Z^e = \begin{pmatrix} I^+ \\ H \\ C \\ D \end{pmatrix}$ , leading to  $Y^e = \begin{pmatrix} Y_1 \\ Y_2 \\ Y_5 \end{pmatrix}$  and

$Z^e = \begin{pmatrix} Z_1 \\ Z_2 \\ Z_3 \\ Z_4 \end{pmatrix}$ . The cascade compartments capturing transition dynamics are expressed as

$G = \begin{pmatrix} Y^G \\ Z^G \end{pmatrix}$  with  $Y^G = \begin{pmatrix} R_2^- \\ V^- \end{pmatrix} = \begin{pmatrix} Y_3 \\ Y_4 \end{pmatrix}$ , while the observable cascade compartments are

given by  $Z^G = (R_1^+, R_2^+, R_3^+, V_1^+, V_2^+, V_3^+)^T = (Z_5, Z_6, Z_7, Z_8, Z_9, Z_{10})^T$ . This refined decomposition explicitly accounts for the hidden compartments  $Y^G$ , further distinguishing them within the cascade dynamics, allowing for a clearer representation of both observed and latent transitions in the model.

The corresponding diffusion approximation follows from Equation (4.1) and is expressed as

$$dX^D(t) = F_{\text{base}}(t, X^D(t))dt + \sigma_{\text{base}}(t, X^D(t))dW(t) + \sum_{k=K+1}^{\bar{K}} \xi_k M_k(t) \quad \text{for } t \in [0, T],$$

where the functions  $F_{\text{base}}$ ,  $\sigma_{\text{base}}$ , and the summation term governing cascade transitions are explicitly provided in Appendix C.2. Based on the discretization approach outlined in Section 4.5.3, and referring to Equation (4.2), the discrete-time version of the model is formulated as

$$X_{n+1} = X_n + F_{\text{base}}(n, X_n)\Delta t + \sigma_{\text{base}}(n, X_n)\sqrt{\Delta t}\mathcal{E}_{n+1} + \sum_{k=K+1}^{\bar{K}} \xi_k M_k(n) \quad \text{for } n \in [0, L],$$

where all associated coefficients are detailed in Appendix C.3. This discrete representation ensures numerical tractability and maintains consistency with the underlying continuous-time stochastic dynamics while integrating the effects of cascade transitions explicitly.

## 5 Data Set and Calibration

In the following sections, we will present a numerical application of the proposed Covid-19 model with cascade states, using real-world data to simulate the spread of the virus and evaluate the effectiveness of different control measures. The model is calibrated using actual epidemiological data from Germany, allowing us to capture approximately the dynamics of infection, recovery, and transmission rates over time.

The calibration process involves adjusting key model parameters such as the transmission rate, test rate, and intervention effectiveness based on historical data. This ensures that the model predictions align with observed trends. By fitting the model to real data, we are able to conduct realistic simulations and evaluate various public health strategies, such as vaccination campaigns, social distancing, and lockdown measures.

Through this application, we aim to demonstrate the practical relevance of the model in predicting the course of the pandemic in the sense of the estimation of the infected non detected for example and providing insights for decision-makers on the most effective ways to mitigate the spread of Covid-19. The results obtained through the calibrated model will be discussed, highlighting how closely the model fits the observed data and the implications for future scenarios.

This section outlines our quantitative understanding of infection spread as reported through testing, focusing on Germany. In Germany, local health authorities collect infection data in accordance with the "Infektionsschutzgesetz (IfSG)" and transmit it to the national public health institute, the "Robert Koch-Institut (RKI)". The primary dataset for our analysis comprises daily incidence figures reported to local health authorities, alongside vaccination data reported to the RKI. Additionally, we incorporate current effective

reproduction number  $\widehat{R}$  value provided by the RKI to provide a comprehensive picture of infection dynamics, from which we can estimate the basic reproduction number  $\widehat{R}_0$  with respect to our model.

The IfSG data published on date  $n$  contains information on cases reported at all previous dates  $n, n-1, \dots, 1$  since the beginning of reporting. However, due to notification delays between testing centers, local health authorities, and the RKI, updating data from date  $n$  not only includes cases reported to local health authorities on date  $n-1$ , but also cases reported on date  $n-1$  and before, on dates  $n-2, n-3, \dots$ , and so forth. This means that the number of cases reported on day  $n$  will be underestimated, particularly for the most recent dates. Significant handling of this data artifact can be done in at least two ways: For example, one may choose to disregard some of the most recent data points, as they are most affected by this data artifact. Another solution is to estimate the systematic discrepancy from datasets published in the past. To prevent prediction bias towards smaller incidences in the forecast, the data can be adjusted accordingly, see Refisch et al. [49]. In this section, we focus on the adjustment of model parameters. We will take the initial approach of ignoring the latest data points, or recognizing that the estimate based on recent points may be underestimated. Consequently, the calibration data extends from the start of the pandemic on March 1, 2020, to February 11, 2023 (approximately 3 years).

## 5.1 Model Parameters

In this section, our aim is to mimic the observed patterns of the Covid-19 pandemic according to the daily new reported case as closely as we can. The calibration method we're introducing here can be viewed as a hybrid approach because it combines real data from the RKI, as mentioned earlier, with the model dynamics and a key parameter of the model. We recognize that one of the most significant parameters in epidemiology is the basic and effective reproduction number. The basic reproduction number (usually denoted by  $\mathcal{R}_0$ ) represents the average number of secondary infections produced by a single infected individual in a susceptible population. It is commonly used metrics to check whether the disease will become an outbreak, and what proportion of the population needs to be vaccinated to eradicate the disease. In fact, at any given time, different proportions of the population are immune to any given disease. For this, the effective reproduction number  $R_e$  is used to quantify the instantaneous spread of disease in the population.

They are fundamental concepts in epidemiology and are used to assess the potential for disease spread within a population. Further, they also help governments to make more accurate epidemic prevention policies. In this section we will consider the deterministic model with the dynamics described by the following

$$d \begin{pmatrix} I^-(t) \\ R^-(t) \\ R^+(t) \\ V(t) \\ S(t) \\ I^+(t) \\ H(t) \\ C(t) \\ D(t) \end{pmatrix} = \begin{pmatrix} \beta \frac{I^-(t)S(t)}{N} - (\alpha + \gamma^+ + \eta^- - \mu)I^-(t) \\ \gamma^- I^-(t) - \mu R^-(t) - \rho_1^- R^-(t) \\ \gamma^+ I^+(t) + \gamma^H H(t) + \gamma^C C(t) - \rho_2^- R^+(t) \\ (I^-(t) + R^-(t) + S(t))\mu - \rho^V V(t) \\ -\beta \frac{I^-(t)S(t)}{N} - \mu S(t) + \rho_1^- R^-(t) + \rho_2^- R^+(t) + \rho^V V(t) \\ \alpha I^-(t) - \eta^+ I^+(t) - \gamma^+ I^+(t) \\ \eta^+ I^+(t) + \eta^- I^-(t) - \delta H(t) - \gamma^H H(t) \\ \delta H(t) - \gamma^C C(t) - \kappa C(t) \\ \kappa C(t) \end{pmatrix} dt$$

**Remark 5.1** The motivation for using the deterministic model for calibration lies in the fact that, under the assumption of a large population size, the ODE limit serves as a good approximation of the stochastic model. This is justified in section 3.1. Additionally, by construction, the stochastic model does not require any new parameters.

The formula of  $\mathcal{R}_0$  is given as follows :

$$\mathcal{R}_0 = \frac{\beta}{\alpha + \gamma^- + \eta^- + \mu} \quad (5.1)$$

Here  $(\alpha + \gamma^- + \eta^- + \mu)^{-1}$  represents the average time before removal from the infectious compartment  $I^-$ . The intuition behind calculating  $\mathcal{R}_0$  here is to compute the inflow into the infectious compartment over the outflow, where the outflow represents the average time before an individual is removed from the infectious compartment  $I^-$  (see [52], [18]). In this formula, we assume that the infection rate  $\beta$ , the test rate  $\alpha$  and the vaccination rate  $\mu$  are time-dependent. In fact, we have several reasons to consider those parameters as time-dependent. First of all, we have the intervention measures by the government. During the Covid-19 pandemic for example, the governments and public health authorities implemented various intervention measures such as social distancing, mask requirements, tests, vaccination campaigns, and travel restrictions. These interventions significantly impact the dynamics of the disease, particularly by altering the contact rate between individuals. They lead to changes in parameters such as the infection rate, which can be viewed as an indicator of the effectiveness of preventive measures, as well as the test rate and vaccination rate. Secondly, the seasonal variability: In general some diseases (Covid-19, flu, cold, etc.) exhibit seasonal patterns in their transmission, influenced by factors such as temperature, humidity, and human behavior. Parameters such as the transmission rate may vary over different seasons, requiring them to be modeled as time-dependent. Another important reason is the emergency of variants due to mutation: With the evolution of the virus, new variants may emerge that affect the transmissibility or severity of the disease. These variants may require adjustments to parameters in the epidemic model to accurately capture their impact on transmission dynamics. In the particular case of the Covid-19 we had in total five notable variants include Alpha, Beta, Gamma, Delta and Omicron variant. All these variants contributed to the changes in the transmission rate. We have also the changes in the behavior: people's behavior and adherence to preventive measures can change over time in response to factors such as changing perceptions of risk, fatigue from prolonged restrictions, or changes in government messaging also change in the weather. These behavioral changes can influence parameters such as contact rates. Finally the heterogeneity in population. The susceptibility of the population, contact patterns, and healthcare capacity

may vary over time due to factors such as population mobility, demographic changes, or the progression of the epidemic itself. Accounting for these time-dependent variations can improve the accuracy of the model's predictions.

Now we consider that in Equation (5.1), the recovery rate  $\gamma^\pm = \frac{1}{14}$ . This indicates that, in the case of Covid-19, an individual who contracts the virus will, on average, take 14 days to recover. For other model parameters, see Table 6.1. At a given time  $n$  the dynamic of  $\mathcal{R}_{0,n}$  is given as

$$\mathcal{R}_{0,n} = \frac{\beta_n}{\alpha_n + \gamma^- + \eta^- + \mu_n}$$

Now, considering a day as the unit of time, we transform the previous system of ordinary differential equations into a discrete-time difference equation system. Using  $\Delta = 1$  and applying a forward finite differences scheme first and introduce cascade states, which results in the system (5.4). The approximate solution of this system can be derived and let  $X_n^\infty$  be that solution. In order to approximate the test rate  $\alpha_n$ , the vaccination rate  $\mu_n$  and the infection rate  $\beta_n$  we consider the Equations from system (5.4) and we have

$$\begin{aligned} I_{n+1}^+ - I_n^+ &= \alpha_n I_n^- - \eta^+ I_n^+ - \gamma^+ I_n^+ \\ V_{1,n+1} - V_{1,n} &= -\psi_1 V_{1,n} + (S_n + I_n^- + R_{1,n}^-) \mu_n \end{aligned}$$

The right hand side represents respectively the daily number of new detected infected individuals which we will denote  $\Delta I_n^+$  and the daily number of new vaccinated individuals denoted as  $\Delta V_n$ .

$$\begin{pmatrix} I_{n+1}^- \\ R_{1,n+1}^- \\ R_{2,n+1}^- \\ V_{n+1}^- \\ S_{n+1} \\ I_{n+1}^+ \\ H_{n+1} \\ C_{n+1} \\ D_{n+1} \\ R_{1,n+1}^+ \\ R_{2,n+1}^+ \\ R_{3,n+1}^+ \\ V_{1,n+1} \\ V_{2,n+1} \\ V_{3,n+1} \end{pmatrix} = \begin{pmatrix} I_n^- \\ R_{1,n}^- \\ R_{2,n}^- \\ V_n^- \\ S_n \\ I_n^+ \\ H_n \\ C_n \\ D_n \\ R_{1,n}^+ \\ R_{2,n}^+ \\ R_{3,n}^+ \\ V_{1,n} \\ V_{2,n} \\ V_{3,n} \end{pmatrix} + \begin{pmatrix} \beta_n \frac{I_n^- S_n}{N} - (\alpha_n + \gamma^+ + \eta^- - \mu_n) I_n^- \\ \gamma^- I_n^- - \mu_n R_{1,n}^- - \rho_1^- R_{1,n}^- \\ -\rho_2^- R_{2,n}^- + \psi_3 R_{3,n}^+ \\ -\rho^V V_n^- + \psi_3 V_{3,n} \\ -\beta_n \frac{I_n^- S_n}{N} - \mu_n S_n + \rho_1^- R_{1,n}^- + \rho_2^- R_{2,n}^- + \rho^V V_n^- \\ \alpha_n I_{n+1}^- - \eta^+ I_n^+ - \gamma^+ I_n^+ \\ \eta^+ I_n^+ + \eta^- I_{n+1}^- - \delta H_n - \gamma^H H_n \\ \delta H_n - \gamma^C C_n - \kappa C_n \\ \kappa C_n \\ \gamma^+ I_n^+ + \gamma^H H_n + \gamma^C C_n - \psi_1 R_{1,n}^+ \\ \psi_1 R_{1,n}^+ - \psi_2 R_{2,n}^+ \\ \psi_2 R_{2,n}^+ - \psi_3 R_{3,n}^+ \\ (I_n^- + R_{1,n}^- + S_n) \mu_n - \psi_1 V_{1,n} \\ \psi_1 V_{1,n} - \psi_2 V_{2,n} \\ V_{2,n} - \psi_3 V_{3,n} \end{pmatrix} \quad (5.4)$$

Then we are going to use the following three main relations in order to estimate the test rate, the vaccination rate and the infection rate.

$$\begin{aligned} \Delta I_n^+ &= \hat{\alpha}_n I_n^- - (\eta^+ + \gamma^+) I_n^+ \\ \Delta V_{1,n} &= (I_n^- + S_n + R_{1,n}^-) \hat{\mu}_n - \psi_1 V_{1,n} \end{aligned}$$

$$\widehat{\mathcal{R}}_0^n = \frac{\widehat{\beta}_n}{(\gamma^- + \widehat{\alpha}_n + \eta^- + \widehat{\mu}_n)}$$

The observed time series of  $\Delta I_n^+$ ,  $\Delta V_n$ ,  $\widehat{\mathcal{R}}_0^n$  is then used to estimate the daily values of transmission rate, test rate, and vaccination rate.

Given the historical data from a certain period ( $0 \leq n \leq L-1$ ), the following algorithm shows how to measure the corresponding  $\beta_n, \alpha_n, \mu_n$  based on the relation above coupled with the equation of the discrete time model.

---

**Algorithm 5.1** Time-Dependent Parameter Estimation
 

---

**Data:**  $\Delta I_n^+, \widehat{\mathcal{R}}_{0,n}, \Delta V_n, 0 \leq n \leq L-1$

**Input:**  $X_0^\infty, \eta^\pm, \gamma^\pm, \gamma^H, \gamma^C, \delta, \kappa, \rho^V, \rho_1^-, \rho_2^-, d_1, d_2$

**Output:**  $\widehat{\alpha}_n, \widehat{\beta}_n, \widehat{\mu}_n, 0 \leq n \leq L-1$

**Initialization**  $n := 0; X_n^\infty := X_0^\infty, \widehat{\alpha}_0, \widehat{\beta}_0, \widehat{\mu}_0$

**for**  $n := 1$  **to**  $L-1$  **do**

Compute  $\overline{X}_n^\infty$  using (5.4)

Use  $\overline{X}_n^\infty$  to update  $\widehat{\alpha}_n, \widehat{\beta}_n, \widehat{\mu}_n$

$$\widehat{\alpha}_n = d_1 \frac{\Delta I_n^+ + (\eta^+ + \gamma^+) I_n^+}{I_n^-}$$

$$\widehat{\mu}_n = d_2 \frac{\Delta V_n + \psi_1 V_n}{(I_n^- + S_n + R_n)}$$

$$\widehat{\beta}_n = \widehat{\mathcal{R}}_0^n (\gamma^- + \widehat{\alpha}_n + \eta^- + \widehat{\mu}_n)$$

**end**

---

**Remark 5.2** In the Algorithm 5.1,  $d_1$  and  $d_2$  are tuning parameters. They are not directly learned from the data during the training process; rather, they need to be set manually to improve the algorithm's effectiveness.

Due to the time series which contains noise, observation errors, the daily estimates of the three driving parameters are also stochastic. It is therefore necessary to smooth or filter the noise in these estimates to obtain robust predictions. Without assuming a specific underlying model for noise, we decided to apply a finite impulse response (FIR) filter to improve the robustness of our predictions. Denote by  $\widetilde{\beta}_n, \widetilde{\alpha}_n, \widetilde{\mu}_n$  the predicted transmission rate, test rate and vaccination rate. From the FIR filters, they are predicted as follows :

$$\widetilde{\beta}_n = \sum_{j=1}^{J_1} a_j \widehat{\beta}_{(n-j)} + a_0 \quad (5.8)$$

$$\widetilde{\alpha}_n = \sum_{l=1}^{J_2} b_l \widehat{\alpha}_{(n-l)} + b_0 \quad (5.9)$$

$$\widetilde{\mu}_n = \sum_{m=1}^{J_3} c_m \widehat{\mu}_{(n-m)} + c_0 \quad (5.10)$$

where  $J_1, J_2$  and  $J_3$  are the orders of the three FIR filters ( $0 < J_1, J_2, J_3 < L-1$ ),  $a_j, j = 1, \dots, J_1, b_l, l = 1, \dots, J_2$  and  $c_m, m = 1, \dots, J_3$  are the coefficients of the impulse responses

of these three FIR filters.

Numerous machine learning techniques, including ordinary least squares (OLS), ridge regression, etc., can be employed to estimate FIR filter coefficients ([43],[14]). This study opts for ridge regression, a method that addresses the following optimization problem:

$$\min_{a_j} \sum_{n=J_1}^{L-1} (\hat{\beta}_n - \tilde{\beta}_n)^2 + \bar{\alpha}_1 \sum_{j=0}^{J_1} a_j^2 \quad (5.11)$$

$$\min_{b_l} \sum_{n=J_2}^{L-1} (\hat{\alpha}_n - \tilde{\alpha}_n)^2 + \bar{\alpha}_2 \sum_{l=0}^{J_2} b_l^2 \quad (5.12)$$

$$\min_{c_m} \sum_{n=J_3}^{L-1} (\hat{\mu}_n - \tilde{\mu}_n)^2 + \bar{\alpha}_3 \sum_{m=0}^{J_3} c_m^2 \quad (5.13)$$

where  $\bar{\alpha}_1, \bar{\alpha}_2$  and  $\bar{\alpha}_3$  are the regularization parameters.

One motivation for using ridge regression instead of OLS is that OLS estimates can have high variance, especially when predictors are highly correlated (multicollinearity) or when the sample size is small relative to the number of predictors. To address this issue, a penalty ( $\bar{\alpha}_1, \bar{\alpha}_2, \bar{\alpha}_3$ ) is added to the regression coefficients, which reduces their magnitude and, consequently, their variance. Ridge regression, also known as  $L_2$  regularization, is one technique used for this purpose.

Now,  $J_1, J_2$  and  $J_3$  was set to 7 since during the Covid-19 pandemic, the data often shows a weekly pattern due to varying reporting practices and behaviors on different days of the week. For example, testing and reporting might be lower on weekends and higher on weekdays. A 7-day period captures this inherent weekly cycle.

## 5.2 Model Prediction

In this subsection, we show how we use the three FIR filters to build model prediction for infection rate, test rate and vaccination rate. Given a period of historical data  $\Delta I_n^+, \hat{R}_{0,n}, \Delta V_n, 0 \leq n \leq L-1$ , we first estimate  $\hat{\beta}_n, \hat{\alpha}_n$  and  $\hat{\mu}_n, 0 \leq n \leq L-1$  by using the Algorithm 5.1. Then we solve the ridge regression with the objective function in (5.11), (5.12), (5.13) and the constraints in (5.8), (5.9),(5.10) to learn the coefficient of the FIR filters, ie.,  $a_j, j = 1, \dots, J_1, b_l, l = 1, \dots, J_2$  and  $c_m, m = 1, \dots, J_3$ . Once we learn these coefficients using a numerical approach, we can obtain the model prediction  $\tilde{\beta}_n, \tilde{\alpha}_n$  and  $\tilde{\mu}_n$ , at time  $L-2$  and compute the prediction at time  $L-1$  by the obtained trained ridge regression in (5.8), (5.9), (5.10).

The specifics of our estimation-prediction method are presented in the following Algorithm. It's important to remind that our deterministic epidemic model relies on the assumption of large population size which lead to  $X_n^\infty$ . This approximation is a consequence of the law of large numbers as describe in Section 3. Consequently, when the population size in each compartment is relatively small, the approximation might not yield accurate results. In such scenarios, stochastic epidemic models could be more suitable.

**Remark 5.3** The estimations obtained from this model will be integrated into our stochastic epidemic model to generate observations for use in our EKF. Additionally, by using

**Algorithm 5.2** Model Prediction for  $\beta_n, \alpha_n, \mu_n$ **Data:**  $\Delta I_n^+, \widehat{R}_{0,n}, \Delta V_n, 0 \leq n \leq L-1$ **Input:**  $X_0^\infty, \eta^\pm, \gamma^\pm, \gamma^H, \gamma^C, \delta, \kappa, \rho^V, \rho_1^-, \rho_2^-, d_1, d_2$ **Output:**  $\widetilde{\alpha}_n, \widetilde{\beta}_n, \widetilde{\mu}_n, 0 \leq n \leq L-1$ **Initialization**  $n := 0; X_n^\infty := X_0^\infty, \widehat{\alpha}_0, \widehat{\beta}_0, \widehat{\mu}_0$ **for**  $n := 1$  *to*  $L-1$  **do**    Compute  $X_n^\infty$  using (5.4)    Use  $X_n^\infty$  to update  $\widehat{\alpha}_n, \widehat{\beta}_n, \widehat{\mu}_n$ 

$$\widehat{\alpha}_n = d_1 \frac{\Delta I_n^+ + (\eta^+ + \gamma^+) I_n^+}{I_n^-}$$

$$\widehat{\mu}_n = d_2 \frac{\Delta V_n + \psi_1 V_n}{(I_n^- + S_n + R_n^-)}$$

$$\widehat{\beta}_n = \widehat{\mathcal{R}}_0^n (\gamma^- + \widehat{\alpha}_n + \eta^- + \widehat{\mu}_n)$$

**end**

Train the ridge regression using (5.11) - (5.12) - (5.13)

Estimate  $\widetilde{\alpha}_{(L-1)}, \widetilde{\mu}_{(L-1)}$  and  $\widetilde{\beta}_{(L-1)}$  by (5.8) - (5.9)- (5.10)

the model's estimation of infection rate, test rate, and vaccination rate, we can estimate the number of detected infected individuals. This allows us to predict the "dark figure" (non-detected infected individuals) within a time window  $[0, L-1]$ .

## 6 Numerical Results

Here we present in-depth numerical analysis of the prediction method we proposed for estimating time-dependent infection, testing, and vaccination rates. In this section, we use the daily reported number of infected individuals in Germany from the beginning of March 2020 through February 2023 as our benchmark. Based on the RKI dataset for daily new infections within this period, we observe the following:

In Figure 6.1, the gray line represents the daily reported new cases in Germany, while the cyan line shows the 7-day moving average applied to this daily data. The calibration process we will discuss primarily focuses on these daily new cases, referred to here as "new arrivals of detected infections." This data will be used to calibrate the time-dependent parameter for the testing rate. Additionally, we will require time series data on vaccinated individuals, not distinguishing between first and second doses. For our purposes, we assume that the vaccinated compartment includes all individuals who have received at least one dose of a Covid-19 vaccine, which will be used for the calibration of the vaccination rate. Finally, we'll use RKI's time-series estimates of the number of basic reproductions to help calibrate the infection rate.

### 6.1 Model Calibration

In this subsection, we solve the optimization problem in Equations (5.11)-(5.13) numerically. To begin, we consider our proposed model 5.4 with the following initial values :



## Daily New Cases in Germany

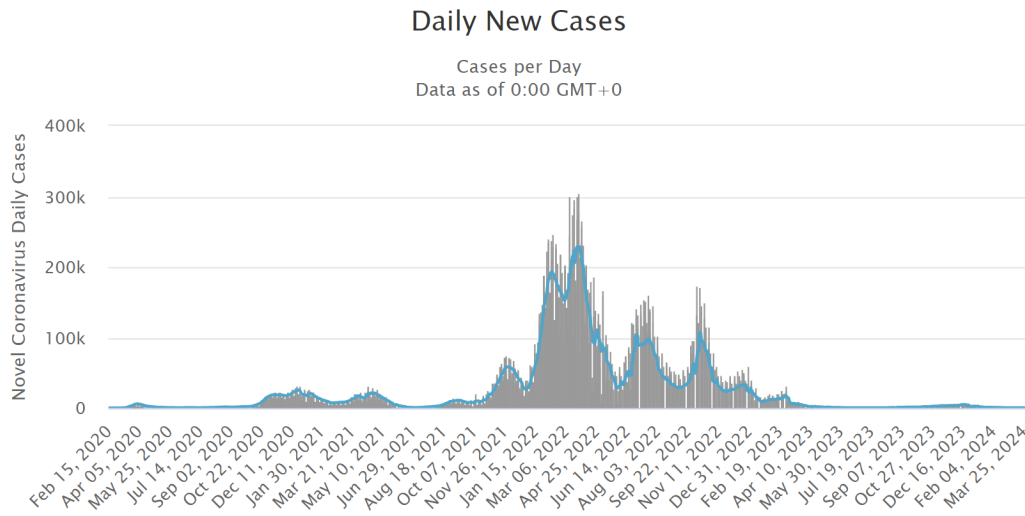


Fig. 6.1: Daily new cases in Germany from February 15, 2020 to March 05, 2024.  
 Source : <https://www.worldometers.info/coronavirus/country/germany/>

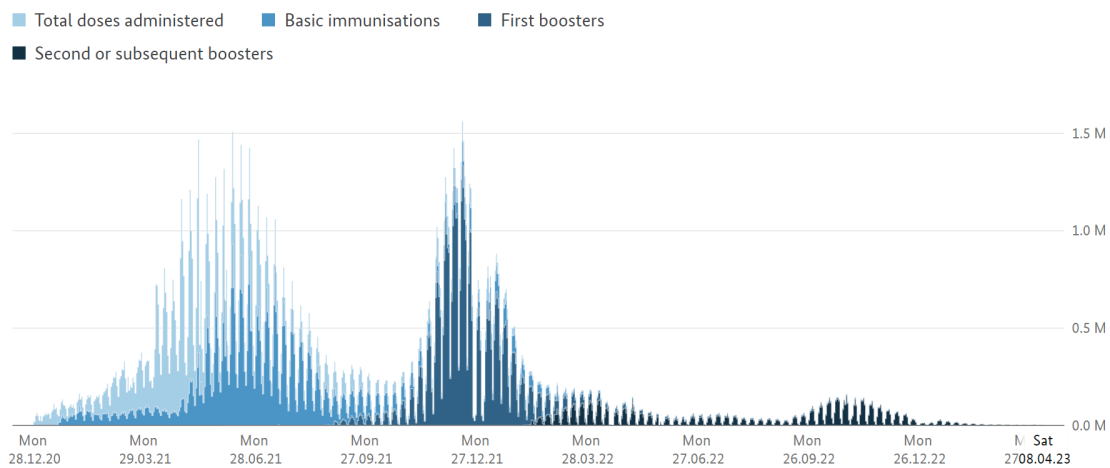


Fig. 6.2: Daily new vaccinated in Germany from December 28, 2020 to April 08, 2023.  
 Source : [impfdashboard.de](http://impfdashboard.de), Robert Koch Institute, Federal Ministry of Health.

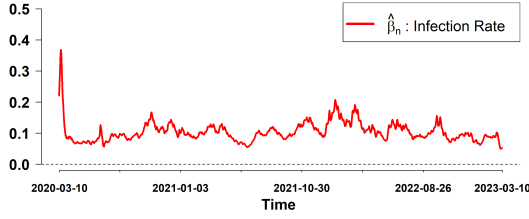
$I_0^+ = 750$  (RKI data),  $R_{1,0}^+ = 331$  (RKI data). We assume that undetected cases (infected or recover) could have been 5 times higher than confirmed cases. This means that according to our model  $I_0^- = 3785$ ,  $R_{1,0}^- = V_0^- = 0$  and  $R_{2,0}^- = 1655$ . We set  $V_{1,0} = V_{2,0} = V_{3,0} = R_{2,0}^+ = R_{3,0}^+ = 0$ . In addition  $H_0 = 184, C_0 = 200, D_0 = 23$ . The model parameters are given in table 6.1.

Next, we apply Algorithm 5.1 to compute  $\hat{\alpha}_n, \hat{\beta}_n,$  and  $\hat{\mu}_n$  for  $n = 1, \dots, L - 1$ . The outputs below illustrate the time-dependent infection rate, test rate, and vaccination rate.

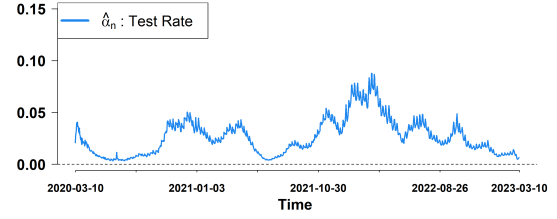
We then fit the resulting time series data to a model using ridge regression. Fitting these data to different models is motivated by the aim to gain insights, make predictions, support

Table 6.1: Parameters values for the Covid-19 model with cascade states. Individuals rates are given.

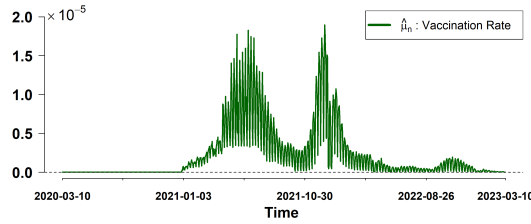
Parameters	Description	Value	Reference
$\mu$	Vaccination rate	$\tilde{\mu}$	Fitted
$\beta$	Transmission rate	$\tilde{\beta}$	Fitted
$\gamma^-$	Recovery rate (for non-detected infected)	0.07	Based on [11]
$\gamma^+$	Recovery rate (for detected infected)	0.07	Based on [11]
$\gamma^H$	Recovery rate from hospitalization	0.048	Based on [13]
$\gamma^C$	Recovery rate from ICU	0.02	Assumed
$\alpha$	Test rate	$\tilde{\alpha}$	Fitted
$\eta^+$	Hospitalized rate (for detected infected)	0.0023	Based on [13]
$\eta^-$	Hospitalized rate (for non-detected infected)	0.0023	Based on [13]
$\delta$	Transfer rate to ICU (for non-detected infected)	0.03	Assumed
$\kappa$	Death rate	0.05	Assumed
$\rho_1^-$	Rate of losing immunity (for Recovered non-detected)	0.01	Assumed
$\rho_2^-$	Rate of losing immunity (for Recovered partially-detected)	0.03	Assumed
$\rho^V$	Rate of losing immunity (after vaccination)	0.005	Assumed



(a) "Noisy" time dependent infection rate estimation



(b) "Noisy" time dependent test rate estimation



(c) "Noisy" time dependent vaccination rate estimation

Fig. 6.3: Estimation infection rate  $\hat{\beta}_n$ , test rate  $\hat{\alpha}_n$  and vaccination rate  $\hat{\mu}_n$ .

data-driven decisions, and better understand the underlying data dynamics over time.

For solving the optimization problems in (5.11)-(5.13), we assume that the response variables  $\tilde{\alpha}_n$ ,  $\tilde{\beta}_n$ , and  $\tilde{\mu}_n$  for  $n = 1, \dots, L-1$  are continuous and follow a Gaussian (normal) distribution. Using the glmnet package in R, we can solve Equations (5.11)-(5.13), yielding

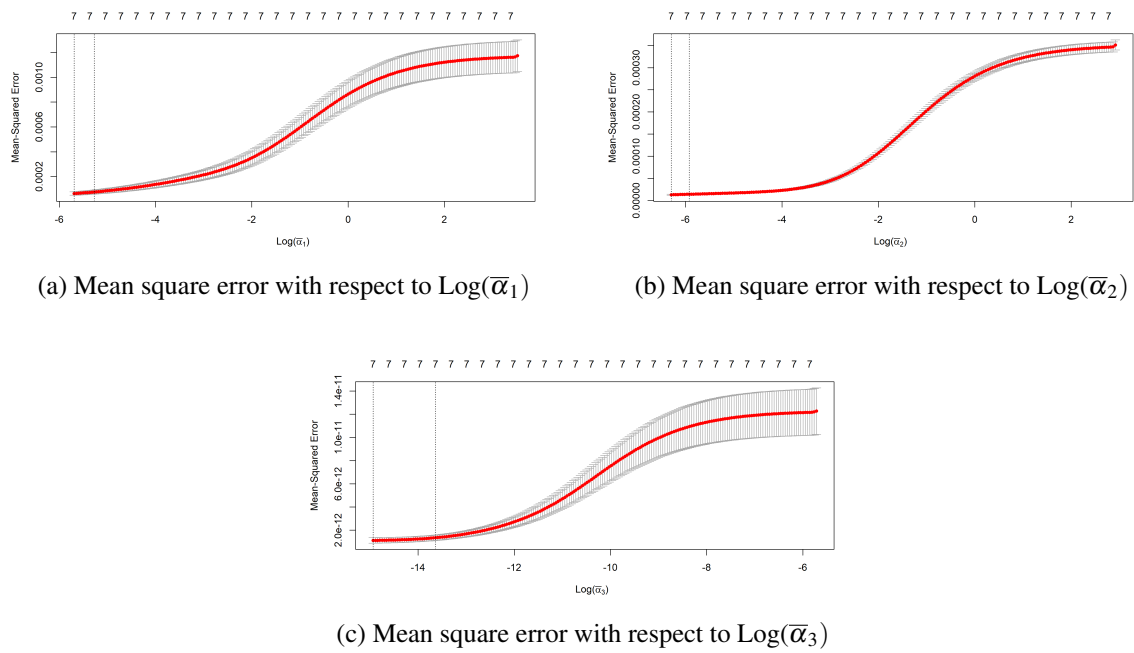


Fig. 6.4: Cross-validation curve (red dotted line) with upper and lower standard deviation bounds along  $\bar{\alpha}_2$  and  $\bar{\alpha}_2$  sequences respectively.

a model prediction for the infection, test, and vaccination rates. First, we split our data ( $\hat{\beta}_n$ ,  $\tilde{\alpha}_n$ , and  $\tilde{\mu}_n$  for  $n = 1, \dots, L - 1$ ) into two distinct subsets: a training set and a testing set. We allocate 70% of the data to the training set and the remaining 30% to the testing set. This division applies to the entire dataset based on the different estimated parameters. We need to provide to the model the value for  $\bar{\alpha}_i, i = 1, 2, 3$ . While the regression coefficient with respect to the three model ( $\tilde{\beta}_n, \tilde{\alpha}_n$  and  $\tilde{\mu}_n$ ) are model-estimated parameters,  $\bar{\alpha}_i, i = 1, 2, 3$  is instead what we call a hyperparameter. It is a parameter that is used to control the training of the model, rather than one that is output in the model-training process. So how do we choose  $\bar{\alpha}_i, i = 1, 2, 3$  with respect to each model?

Typically, we use cross-validation to find the regularization parameter that generates the best-fitting model. Fortunately, the glmnet package can do this automatically. After running the ridge regression we obtain the following Figures (6.4a,6.4b,6.4c) which illustrate the cross-validation. The graph (6.4a,6.4b and 6.4c) illustrates the cross-validation process for Ridge regression, showing the relationship between the regularization parameter  $\bar{\alpha}_i, i = 1, 2, 3$  and the mean square error (MSE) over several folds. The x-axis represents the log values of the regularization parameters  $\text{log}(\bar{\alpha}_i), i = 1, 2, 3$  while the y-axis displays the corresponding mean square error. As a reminder, a low mean squared error indicates better fit. The upper part of the graph shows the number of effective variables (non-zero coefficients) included in the model for each value of  $\bar{\alpha}_i, i = 1, 2, 3$ . The solid curve represents the cross-validated mean MSE, and the surrounding shaded area represents the standard error. Two particular values are marked with dotted vertical lines. The first is the  $\bar{\alpha}_1$  value that resulted in the lowest mean-squared error (called lambda.min by the package). The second is the largest value of  $\bar{\alpha}_1$  that provides cross-validated error within one standard error of the minimum (called lambda.1se). We often are more interested in this latter value

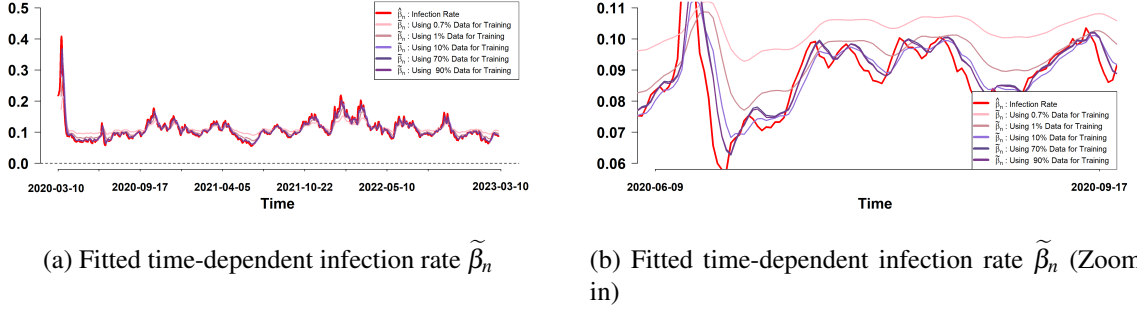


Fig. 6.5: Estimation of  $\tilde{\beta}_n$  using ridge regression, relative to the proportion of data allocated for model training.

than the former, as one goal of these methods is to prevent over-fitting. Thus, we are often willing to sacrifice some goodness of fit for the sake of greater regularization.

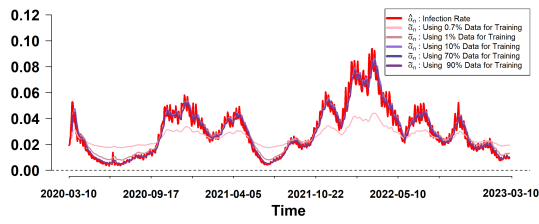
With this in mind, let's choose the model generated with a lambda equal to lambda.1se as the model we want to go with. We can now test this model on our test dataset by computing model-predicted values for the test dataset and computing the mean square error. The obtained models prediction according to the estimated coefficient is given in (6.1), (6.2), (6.3).

$$\begin{aligned}
 \tilde{\beta}_n &\approx \sum_{j=1}^J \tilde{a}_j \hat{\beta}_{(n-j)} + a_0 \\
 &= 0.533 \hat{\beta}_{(n-1)} + 0.250 \hat{\beta}_{(n-2)} + 0.080 \hat{\beta}_{(n-3)} + 0.012 \hat{\beta}_{(n-4)} \\
 &\quad + 0.009 \hat{\beta}_{(n-5)} + 0.017 \hat{\beta}_{(n-6)} + 0.013 \hat{\beta}_{(n-7)} + 0.01
 \end{aligned} \tag{6.1}$$

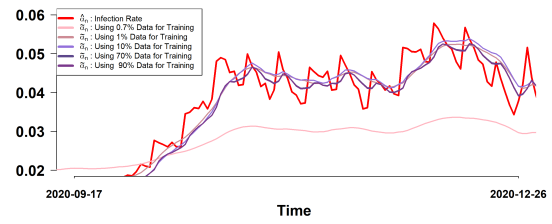
$$\begin{aligned}
 \tilde{\alpha}_n &\approx \sum_{j=1}^J \tilde{a}_j \hat{\alpha}_{(n-j)} + a_0 \\
 &= 0.278 \hat{\alpha}_{(n-1)} + 0.142 \hat{\alpha}_{(n-2)} + 0.075 \hat{\alpha}_{(n-3)} + 0.061 \hat{\alpha}_{(n-4)} \\
 &\quad + 0.086 \hat{\alpha}_{(n-5)} + 0.154 \hat{\alpha}_{(n-6)} + 0.18 \hat{\alpha}_{(n-7)} + 0.001
 \end{aligned} \tag{6.2}$$

$$\begin{aligned}
 \tilde{\mu}_n &\approx \sum_{j=1}^J \tilde{a}_j \hat{\mu}_{(n-j)} + a_0 \\
 &= 0.270 \hat{\mu}_{(n-1)} + 0.0773 \hat{\mu}_{(n-2)} - 0.0830 \hat{\mu}_{(n-3)} - 0.018 \hat{\mu}_{(n-4)} \\
 &\quad + 0.088 \hat{\mu}_{(n-5)} + 0.021 \hat{\mu}_{(n-6)} + 0.294 \hat{\mu}_{(n-7)} + 2 \times 10^{-6}
 \end{aligned} \tag{6.3}$$

At this stage, we can apply the obtained model predictor to filter out noise from  $\hat{\beta}_n$ . Figures 6.5a and 6.5b show that increasing the amount of training data improves the model's estimation accuracy. Based on these figures, using 70% of the "noisy" data (specifically,  $\hat{\beta}_n$ ) is sufficient for the model to produce a good approximation in terms of MSE. Beyond 70% of data for training, we observe a convergence, as outputs become nearly indistinguishable. We now apply this methodology to the time series for the test rate,  $\hat{\alpha}_n$ , and the vaccination rate,  $\hat{\mu}_n$ . The following images illustrate our results.

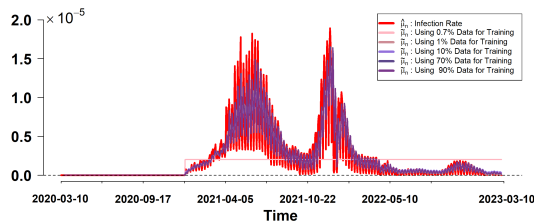


(a) Fitted time-dependent infection rate  $\tilde{\alpha}_n$

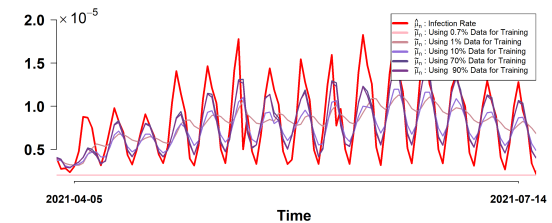


(b) Fitted time-dependent infection rate  $\tilde{\alpha}_n$  (Zoom in)

Fig. 6.6: Estimation of  $\tilde{\alpha}_n$  using ridge regression, relative to the proportion of data allocated for model training.

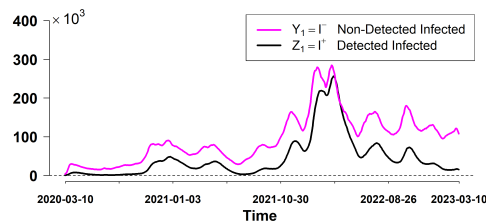


(a) Fitted time-dependent infection rate  $\tilde{\mu}_n$

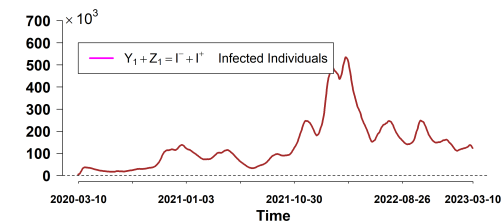


(b) Fitted time-dependent infection rate  $\tilde{\mu}_n$  (Zoom in)

Fig. 6.7: Estimation of  $\tilde{\mu}_n$  using ridge regression, relative to the proportion of data allocated for model training.



(a) Dynamic of infected detected/non-detected individuals

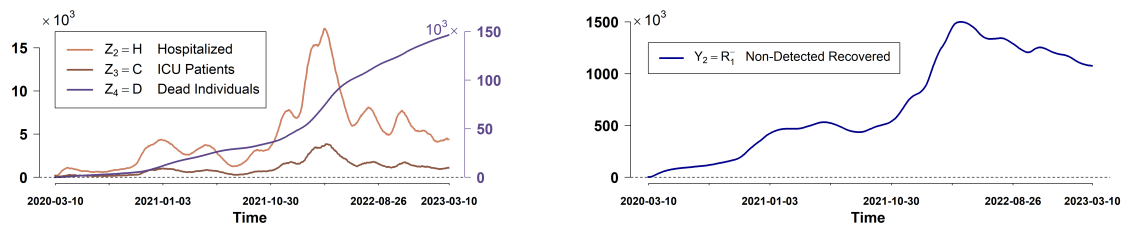


(b) Dynamic of total infected individuals

Fig. 6.8: Dynamics of Infected individuals.

## 6.2 Simulation of Covid-19 Model

In this section, we simulate the proposed Covid-19 model using parameters derived from two sources: the regression analysis results outlined in the previous subsection 6.1 and values presented in Table 6.1. The initial conditions are detailed in Subsection 6.1. The following Figures (6.8a-6.8b) illustrates the dynamics of infected individuals over time.



(a) Dynamic of Hospitalized, ICU and Dead individuals.

(b) Dynamic of non detected recovered individuals

Fig. 6.9: Dynamics of Hospitalization, ICU, Dead individuals/ Recovered non-detected.

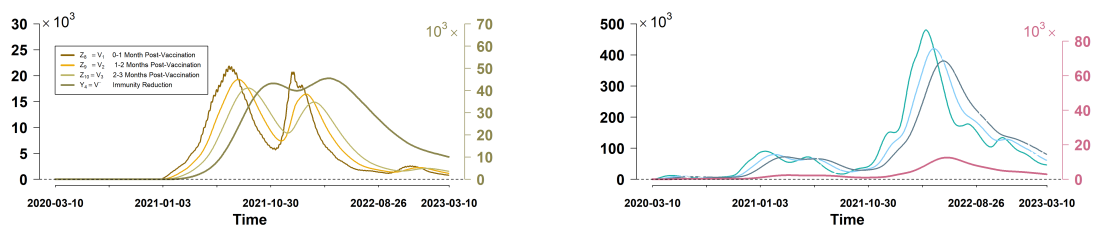


Fig. 6.10: Dynamics of vaccinated/recovered individuals

The left panel 6.8a displays the number of detected and non-detected infections and the right panel 6.8b, shows the cumulative number of infections, calculated as the sum of detected and undetected cases. The overall trend closely resembles the reported detected cases in Germany during the same period 6.2 . Furthermore, the model estimates the number of non-detected cases over time. This information, unavailable during the pandemic, could provide valuable decision-making insights.

The model also visualizes additional metrics, such as the number of ICU patients and deaths (Fig. 6.9a). Notably, the model considers deaths only from ICU cases, reflecting the situation in Germany and other developed countries. Based on the graph 6.8a, it is evident that around May 2022, the estimated number of undetected infections diverged from the curve of detected infections. This shift could be attributed to the intensive vaccination campaign in Germany at that time. The combination of high vaccination rates 6.3b and robust testing 6.3c significantly reduced the number of undetected cases. However, by the summer of the same year, the number of undetected cases began to rise noticeably. This increase may be due to a considerable reduction in both testing and vaccination efforts.

The inclusion of cascading compartments enables us to track the progression of recovered (or vaccinated) individuals across various stages until their eventual transition into the compartments of recovered (or vaccinated) individuals with fading immunity (see Figure 6.10).

Now, we shift our attention to individuals who recovered from the disease without being identified or detected as infected. By monitoring non-detected infections 6.8a and their subsequent recovery 6.9b, we can uncover the hidden dynamics of disease spread, which is often underestimated in real-world reports. This information is highly valuable

for public health strategies, as it helps identify the extent of non-detected cases that could silently continue propagating the infection within the population.

## 7 Conclusion

This study introduces a stochastic epidemic model framed within a continuous-time Markov chain (CTMC), effectively bridging theoretical foundations and practical application. By incorporating Poisson processes to model transitions and cascade states to manage partially hidden compartments, the approach provides a robust structure for analyzing complex epidemiological dynamics. The application of the random time change theorem and the derivation of a diffusion approximation via the central limit theorem highlight the model's analytical depth.

Adaptation of the framework to Covid-19 demonstrates its versatility and relevance, showcasing its ability to integrate real-world data for parameter estimation and calibration. Overall, this model offers a powerful tool for understanding epidemic processes, predicting disease trends, and informing public health strategies, particularly in the context of infectious disease outbreaks.

**Acknowledgments** The authors thank Olivier Menoukeu Pamen (University of Liverpool), Gerd Wachsmuth, Armin Fügenschuh, Markus Friedemann, Jesse Beisegele (BTU Cottbus–Senftenberg) for insightful discussions and valuable suggestions that improved this paper.

**Funding** The authors gratefully acknowledge the support by the Deutsche Forschungsgemeinschaft (DFG), award number 458468407, and by the German Academic Exchange Service (DAAD), award number 57417894.

## A List of Abbreviations

SIR	Susceptible Infected Recovered (with long life immunity)
SIRS	Susceptible Infected Recovered (with loss of immunity)
SIERV	Susceptible Infected Exposed Recovered Vaccination
Covid-19	Coronavirus Disease 2019
ODE	Ordinary Differential Equation
SDE	Stochastic Differential Equation
CTMC	Continuous Time Markov Chain
HCTMC	Homogeneous Continuous Time Markov Chain
CTMC	Non-Homogeneous Continuous Time Markov Chain
LLN	Law of Large Number
CLT	Central Limit Theorem
EKF	Extended Kalman Filter
$SI^{\pm}RS$	Susceptible Infected detected/non-detected Recovered (with loss of immunity)
MOR	Model Order Reduction
POD	Proper Orthogonal Decomposition
SVD	Singular Value Decomposition
ML	Maximum likelihood
OLS	Ordinary Least Square
FIR	Finite Impulse Response

**B List of Notations**

$\alpha$	Test rate
$\beta$	Transmission rate
$\gamma$	Recovered rate
$\delta$	Hospitalization rate in the iCU
$\eta^- / \eta^+$	Hospitalization rate from non-detected / detected infected individuals
$\mathcal{R}_0$	Basic reproduction number
$\kappa$	Death rate from ICU
$\lambda = \lambda(t, X(t))$	intensity rate
$\mu$	Vaccination rate
$\nu$	Intensity rate according to $\bar{X}$
$\upsilon$	Infection rate from $E$ to $I^-$
$\rho$	Losing immunity rate
$\sigma$	Diffusion coefficient for diffusion approximation of CTMC $X$
$\bar{\sigma}$	Diffusion coefficient for diffusion approximation of CTMC $\bar{X}$
$\tau = \tau_k(t)$	Time change representation
$\psi_k$	Deterministic transition from one generic compartment to another
$\xi_k$	Transition vector
$\hat{\alpha}$	Test rate approximation
$\hat{\beta}$	Transmission rate approximation
$\hat{\mu}$	Vaccination rate approximation
$\tilde{\alpha}$	Regression model for test rate
$\tilde{\beta}$	Regression model for transmission rate
$\tilde{\mu}$	Regression model for vaccination rate
$C$	Number of individuals in the ICU
$D$	Number of individuals who died from the disease in ICU
$d$	Number of compartment in a given model
$E$	Number of exposed individuals
$F$	Drift coefficient for diffusion approximation for CTMC $X$
$\bar{F}$	Drift coefficient for diffusion approximation for CTMC $\bar{X}$
$G$	Gaussian process
$G_i$	Generique compartment $i$
$H$	Number of hospitalized individuals
$I$	Number of infected individuals
$I^- / I^+$	Number of infected non-detected / detected
$\mathbb{I}_n$	$n \times n$ Identity matrix of order $n$
$K$	total number of different transitions
$\bar{K}$	Total number of group $P_k$
$L$	Total number of time steps
$M_k$	Counting process (counts the number of transition $k$ in $[0, t]$ )
$N$	total population size
$P$	$P \in \mathbb{N}$ of "daily" sub-compartment to one compartment
$\mathbf{P}(t)$	Transition matrix
$Q^G$	Generator matrix
$R$	Number of recovered individuals
$R^-, R^+$	Number of recovered non detected/detected individuals
$R_1^+, R_2^+, R_3^+$	Generic compartment with respect to observable recovered



$V_1, V_2, V_3$	Generic compartment with respect to vaccinated individuals
$S$	Number of susceptible individuals at time $t$
$W$	$K$ -dimensional standard Brownian motions
$X(t)$	State for absolute sub-population size
$\bar{X}(t)$	Relative sub-population size
$Y_k(\cdot)$	Standard Poisson process with unit intensity
$Y$	Hidden state
$Z$	Observable state
$\tilde{Y}$	Hidden state approximation via Taylor expansion
$\bar{Y}$	The value around which we perform the Taylor expansion
$\tilde{Z}$	Observable state approximation via Taylor expansion
$M_n$	Conditional mean in the EKF
$Q_n$	Conditional covariance in the EKF
$\mathbb{F} = \{\mathcal{F}_t\}_{t \geq 0}$	Natural filtration of $X$
$\mathbb{N}$	Set of natural number
$\mathcal{F}_t^X$	Sigma algebra generated by $X$
$\mathbb{P}$	Probability measure on a measurable space $(\Omega, \mathcal{F}_T)$
$\xi_k$	$d$ -dimensional vector formed by 0, 1 and $-1$
$\Omega$	Sample space
$\bar{\tau}$	Waiting time for a CTMC
$f(\cdot)$	Density function
$\bar{F}(\cdot)$	Survival function
$\delta$	Infinitesimal small time
$F(\cdot)$	Cumulative distribution function
$\xi$	Uniform random variable in the Gillespie algorithm
$\mathcal{E}_n^i$	Independent sequence of i.i.d. $\mathcal{N}(0, \mathbb{I})$ Random vector
$\bar{f}$	Drift coefficient of the signal (continuous-time )
$\bar{h}$	Drift coefficient of the observations (continuous-time )
$\bar{\sigma}$	First diffusion coefficient of the signal (continuous-time )
$\bar{g}$	Second diffusion coefficient of the signal (continuous-time )
$\bar{\ell}$	Second diffusion coefficient of the observations (continuous time dynamic)
$f_0, f_1$	Drift coefficient of the signal (discrete-time )
$h_0, h_1$	Drift coefficient of the observations (discrete-time )
$\sigma$	First diffusion coefficient of the signal (discrete-time )
$g$	Second diffusion coefficient of the signal (discrete-time )
$\ell$	Second diffusion coefficient of the observations (discrete-time )
$T$	Time horizon
$T_n$	Time of the $n^{th}$ jump CTMC
$t_n = n\Delta_L$	discrete time points with $L$ the number of time steps
$\Delta_L$	step size, $\Delta_L = T/L = t_{n+1} - t_n$
$V$	Number of vaccinated individuals
$V^-$	Number of vaccinated individuals with fading immunity
$\mathcal{Z}_n$	Whole observation path
$\mathbb{P} - a.s.$	Almost surely with respect to the probability measure $\mathbb{P}$
$\ \cdot\ $	Euclidean norm
$ \cdot $	Absolute value
$J, L, M$	Order of the FIR
$a_j, b_l, c_m$	Impulse response coefficient

$L^G$ 

Total number of cascade states

**C Model Dynamics**Table C.1: Transition vectors and intensities for the cascade state counting process:  $\xi_k$  and  $M_k$ ,  $k = K + 1, \dots, \bar{K}$ 

k	Transition	Transition vectors $\xi_k$	$M_k(X)$
K+1	Transition from $R_1^+$ to $R_2^+$	$(0, 0, 0, 0, 0, 0, 0, 0, 0, 0, -1, 1, 0, 0, 0, 0)^\top$	$\psi_1 R_1^+ = \psi_1 Z_5$
K+2	Transition from $R_2^+$ to $R_3^+$	$(0, 0, 0, 0, 0, 0, 0, 0, 0, 0, -1, 1, 0, 0, 0, 0)^\top$	$\psi_2 R_2^+ = \psi_2 Z_6$
K+3	Transition from $R_3^+$ to $R_2^-$	$(0, 0, 1, 0, 0, 0, 0, 0, 0, 0, 0, 0, -1, 0, 0, 0)^\top$	$\psi_3 R_3^+ = \psi_3 Z_7$
K+4	Transition from $V_1$ to $V_2$	$(0, 0, 0, 0, 0, 0, 0, 0, 0, 0, 0, 0, 0, -1, 1, 0)^\top$	$\psi_1 V_1 = \psi_1 Z_8$
K+5	Transition from $V_2$ to $V_3$	$(0, 0, 0, 0, 0, 0, 0, 0, 0, 0, 0, 0, 0, 0, -1, 1)^\top$	$\psi_2 V_2 = \psi_2 Z_9$
K+6	Transition from $V_3$ to $V^-$	$(0, 0, 0, 1, 0, 0, 0, 0, 0, 0, 0, 0, 0, 0, 0, -1)^\top$	$\psi_3 V_3 = \psi_3 Z_{10}$

$$\begin{aligned} \xi_k M_k = & (0, 0, \psi_3 Z_7, \psi_3 Z_{10}, 0, 0, 0, 0, 0, \\ & - \psi_1 Z_5, \psi_1 Z_5 - \psi_2 Z_6, \psi_2 Z_6 - \psi_3 Z_7, -\psi_1 Z_8, \psi_1 Z_8 - \psi_2 Z_9, \psi_2 Z_9 - \psi_3 Z_{10})^\top \end{aligned}$$







## References

1. AHMAD, M. D., USMAN, M., KHAN, A., AND IMRAN, M. Optimal control analysis of Ebola disease with control strategies of quarantine and vaccination. *Infectious diseases of poverty* 5 (2016), 1–12.
2. AHMAD, W., BUTT, A., RAFIQ, M., ASIF, Z., ISMAEEL, T., AND AHMAD, N. Modeling, analyzing and simulating the Measles transmission dynamics through efficient computational optimal control technique. *The European Physical Journal Plus* 139, 7 (2024), 1–30.
3. AHMAD, Y. U., ANDRAWUS, J., ADO, A., MAIGORO, Y. A., YUSUF, A., ALTHOBAITI, S., AND MUSTAPHA, U. T. Mathematical modeling and analysis of human-to-human monkeypox virus transmission with post-exposure vaccination. *Modeling Earth Systems and Environment* 10, 2 (2024), 2711–2731.
4. ALLEN, L. J. An introduction to stochastic epidemic models. In *Mathematical Epidemiology*, F. Brauer, P. van den Driessche, and J. Wu, Eds., vol. 1945 of *Lecture Notes in Mathematics*. Springer, Berlin, Heidelberg, 2008, pp. 81–130.
5. ALLEN, L. J. Stochastic population and epidemic models. *Mathematical biosciences lecture series, stochastics in biological systems I* (2015), 120–128.
6. ALLEN, L. J., AND LAHODNY JR, G. E. Extinction thresholds in deterministic and stochastic epidemic models. *Journal of biological dynamics* 6, 2 (2012), 590–611.
7. ALLEN, L. J., AND WANG, X. Stochastic models of infectious diseases in a periodic environment with application to cholera epidemics. *Journal of Mathematical Biology* 82, 6 (2021), 48.
8. ANDERSON, D. F., AND KURTZ, T. G. Continuous time Markov chain models for chemical reaction networks. In *Design and analysis of biomolecular circuits*. Springer, 2011, pp. 3–42.
9. BARBAROSSA, M. V., FUHRMANN, J., MEINKE, J. H., KRIEG, S., VARMA, H. V., CASTELLETTI, N., AND LIPPERT, T. Modeling the spread of COVID-19 in germany: Early assessment and possible scenarios. *Plos one* 15, 9 (2020), e0238559.
10. BARDINA, X., FERRANTE, M., AND ROVIRA, C. A stochastic epidemic model of COVID-19 disease. *arXiv preprint arXiv:2005.02859* (2020).
11. BHAPKAR, H., MAHALLE, P. N., DEY, N., AND SANTOSH, K. Revisited COVID-19 mortality and recovery rates: are we missing recovery time period? *Journal of Medical Systems* 44, 12 (2020), 202.
12. BRITTON, T., AND PARDOUX, E., Eds. *Stochastic Epidemic Models with Inference*. Springer Internat. Publ., 2019.
13. CHARPENTIER, A., ELIE, R., LAURIÈRE, M., AND TRAN, V. C. COVID-19 pandemic control: balancing detection policy and lockdown intervention under ICU sustainability, 2020.
14. CHEN, Y.-C., LU, P.-E., CHANG, C.-S., AND LIU, T.-H. A time-dependent sir model for COVID-19 with undetectable infected persons. *Ieee transactions on network science and engineering* 7, 4 (2020), 3279–3294.
15. COLANERI, K., DAMIAN, C., AND FREY, R. Invisible infections: A partial information approach for estimating the transmission dynamics of the Covid-19 pandemic. *arXiv preprint arXiv:2212.13443* (2022).
16. DAYAN, F., AHMED, N., RAFIQ, M., RAZA, A., KHAN, I., AND EL DIN, E. M. T. A reliable numerical investigation of an seir model of measles disease dynamics with fuzzy criteria. *Scientific Reports* 13, 1 (2023), 15840.
17. DIDELOT, X., WHITTLES, L. K., AND HALL, I. Model-based analysis of an outbreak of bubonic plague in cairo in 1801. *Journal of The Royal Society Interface* 14, 131 (2017), 20170160.
18. DIEKMANN, O., HEESTERBEEK, J. A. P., AND METZ, J. A. J. On the definition and the computation of the basic reproduction ratio  $r_0$  in models for infectious diseases in heterogeneous populations. *Journal of mathematical biology* 28 (1990), 365–382.
19. EL BAROUDI, M., LAARABI, H., ZOUHRI, S., RACHIK, M., AND ABTA, A. Stochastic optimal control model for COVID-19: mask wearing and active screening/testing. *Journal of Applied Mathematics and Computing* (2024), 1–31.
20. ETHIER, S. N., AND KURTZ, T. G. *Markov processes: characterization and convergence*. John Wiley & Sons, 2009.
21. FARHAN, M., SHAH, Z., LING, Z., SHAH, K., ABDELJAWAD, T., ISLAM, S., AND GARALLEH, H. A. Global dynamics and computational modeling for analyzing and controlling Hepatitis b: A novel epidemic approach. *Plos one* 19, 6 (2024), e0304375.
22. FERGUSON, N. M., LAYDON, D., NEDJATI-GILANI, G., IMAI, N., AINSLIE, K., BAGUELIN, M., BHATIA, S., BOONYASIRI, A., CUCUNUBÁ, Z., CUOMO-DANNENBURG, G., ET AL. Impact of non-pharmaceutical interventions (npis) to reduce COVID-19 mortality and healthcare demand. imperial college COVID-19 response team. *Imperial College COVID-19 Response Team* 20, 10.25561 (2020), 77482.
23. FINKENSTÄDT, B. F., BJØRNSTAD, O. N., AND GRENFELL, B. T. A stochastic model for extinction and recurrence of epidemics: estimation and inference for measles outbreaks. *Biostatistics* 3, 4 (2002), 493–510.
24. FOOD, U., AND ADMINISTRATION, D. Antibody (serology) testing for COVID-19: Information for patients and consumers, 2024.
25. FOR DISEASE CONTROL, C., AND (CDC), P. Measles, 2024.
26. GILLESPIE, D. T. Exact stochastic simulation of coupled chemical reactions. *The journal of physical chemistry* 81, 25 (1977), 2340–2361.
27. GÜMÜŞ, M., AND TÜRK, K. Dynamical behavior of a hepatitis b epidemic model and its nsfd scheme. *Journal of Applied Mathematics and Computing* (2024), 1–22.
28. GUO, B., KHAN, A., AND DIN, A. Numerical simulation of nonlinear stochastic analysis for measles transmission: A case study of a measles epidemic in pakistan. *Fractal and Fractional* 7, 2 (2023), 130.
29. GUY, R., LARÉDO, C., AND VERGU, E. Approximation of epidemic models by diffusion processes and their statistical inference. *Journal of Mathematical Biology* 70, 3 (2015), 621–646.
30. GUY, R., LARÉDO, C., AND VERGU, E. Approximation and inference of epidemic dynamics by diffusion processes. *Journal de la Société Française de Statistique* 157, 1 (2016), 71–100.
31. HASAN, A., SUSANTO, H., TJAJONO, V., KUSDANTARA, R., PUTRI, E., NURAINI, N., AND HADISOEMARTO, P. A new estimation method for COVID-19 time-varying reproduction number using active cases. *Scientific Reports* 12, 1 (2022), 6675.
32. HE, S., TANG, S., RONG, L., ET AL. A discrete stochastic model of the COVID-19 outbreak: Forecast and control. *Math. Biosci. Eng* 17, 4 (2020), 2792–2804.
33. IBRAHIM, M. A., AND DÉNES, A. Stability and threshold dynamics in a seasonal mathematical model for Measles outbreaks with double-dose vaccination. *Mathematics* 11, 8 (2023), 1791.
34. KERMACK, W. O., AND MCKENDRICK, A. G. A contribution to the mathematical theory of epidemics. *Proceedings of the royal society of london. Series A, Containing papers of a mathematical and physical character* 115, 772 (1927), 700–721.
35. KÖHLER-RIEPEL, F., RÖHL, C. H., AND DE MICHELI, E. A novel deterministic forecast model for the Covid-19 epidemic based on a single ordinary integro-differential equation. *The European Physical Journal Plus* 135, 7 (2020), 599.

36. KURTZ, T. G. Limit theorems for sequences of jump Markov processes approximating ordinary differential processes. *Journal of Applied Probability* 8, 2 (1971), 344–356.
37. KURTZ, T. G. Limit theorems and diffusion approximations for density dependent Markov chains. *Stochastic Systems: Modeling, Identification and Optimization, I* (1976), 67–78.
38. KURTZ, T. G. Strong approximation theorems for density dependent Markov chains. *Stochastic Processes and their Applications* 6, 3 (1978), 223–240.
39. LI, Y., AND WEI, Z. Dynamics and optimal control of a stochastic coronavirus (COVID-19) epidemic model with diffusion. *Nonlinear Dynamics* (2022), 1–30.
40. LIU, G., AND LI, H. Dynamical analysis of a class of Monkeypox epidemic model. *Thermal Science* 28, 4 Part B (2024), 3367–3383.
41. MAMIS, K., AND FARAZMAND, M. Stochastic compartmental models of the COVID-19 pandemic must have temporally correlated uncertainties. *Proceedings of the Royal Society A* 479, 2269 (2023), 20220568.
42. MBOUANDI NJASSE, I., OUBO KAMKUMO, F., AND WUNDERLICH, R. Stochastic optimal control of an epidemic under partial information. *Submitted to arxiv.org* (2025).
43. MICHELETTI, A., FERRARI, L., GERARDI, G., MANZI, G., NICOLUSSI, F., BIGANZOLI, E., AND SALINI, S. Modeling provincial Covid-19 epidemic data using an adjusted time-dependent sird model. In *Proceedings of SIMAI 2020+ 21*. Università di Parma, 2021, pp. 571–572.
44. MINTA, A. A. Progress toward measles elimination—worldwide, 2000–2022. *MMWR. Morbidity and Mortality Weekly Report* 72 (2023).
45. NARCI, R., DELATTRE, M., LARÉDO, C., AND VERGU, E. Inference for partially observed epidemic dynamics guided by Kalman filtering techniques. *Computational Statistics & Data Analysis* 164 (2021), 107319.
46. OUBO KAMKUMO, F., MBOUANDI NJASSE, I., AND WUNDERLICH, R. State estimation in stochastic epidemic models under partial information. *Working paper* (2025).
47. QUALLS, N. Community mitigation guidelines to prevent pandemic influenza—united states, 2017. *MMWR. Recommendations and reports* 66 (2017).
48. QURESHI, M., KHAN, S., BANTAN, R. A., DANIYAL, M., ELGARHY, M., MARZO, R. R., AND LIN, Y. Modeling and forecasting monkeypox cases using stochastic models. *Journal of Clinical Medicine* 11, 21 (2022), 6555.
49. REFISCH, L., LORENZ, F., RIEDLINGER, T., TAUBENBÖCK, H., FISCHER, M., GRABENHENRICH, L., WOLKEWITZ, M., BINDER, H., AND KREUTZ, C. Data-driven prediction of COVID-19 cases in germany for decision making. *BMC medical research methodology* 22, 1 (2022), 116.
50. SONG, J., XIE, H., GAO, B., ZHONG, Y., GU, C., AND CHOI, K.-S. Maximum likelihood-based extended Kalman filter for COVID-19 prediction. *Chaos, Solitons & Fractals* 146 (2021), 110922.
51. TESFAYE, A. W., AND SATANA, T. S. Stochastic model of the transmission dynamics of COVID-19 pandemic. *Advances in Difference Equations* 2021 (2021), 1–21.
52. VAN DEN DRIESCHE, P., AND WATMOUGH, J. Reproduction numbers and sub-threshold endemic equilibria for compartmental models of disease transmission. *Mathematical biosciences* 180, 1-2 (2002), 29–48.
53. ZHU, X., GAO, B., ZHONG, Y., GU, C., AND CHOI, K.-S. Extended Kalman filter based on stochastic epidemiological model for COVID-19 modelling. *Computers in Biology and Medicine* 137 (2021), 104810.